Homeoidally striated density profiles. II. Anisotropy and rotation

R. Caimmi*

February 5, 2008

Abstract

With regard to homeoidally striated Jacobi ellipsoids (Caimmi & Marmo 2005), a unified theory of systematically rotating and peculiar motions is developed, where both real and imaginary rotation (around a fixed axis) are considered. The effect of positive or negative residual motion excess, is shown to be equivalent to an additional real or imaginary rotation, respectively. Then it is realized that a homeoidally striated Jacobi ellipsoid with assigned velocity distribution, always admits an adjoint configuration i.e. a classical Jacobi ellipsoid of equal mass and axes. In addition, further constraints are established on the amount of residual velocity anisotropy along the principal axes, for triaxial configurations. Special effort is devoted to investigating sequences of virial equilibrium configurations in terms of normalized parameters, including the effects of both density and velocity profile. In particular, it is shown that bifurcation points from axisymmetric to triaxial configurations occur as in classical Jacobi ellipsoids, contrary to earlier results (Wiegandt 1982a,b; Caimmi & Marmo 2005). The reasons of the above mentioned discrepancy are also explained.

*Astronomy Department, Padua Univ., Vicolo Osservatorio 2, I-35122 Padova, Italy
email: caimmi@pd.astro.it

The occurrence of centrifugal support at the ends of major equatorial semiaxis, is briefly discussed. An interpretation of recent results from numerical simulations on stability (Meza 2002), is provided in the light of the model. A physical interpretation of the early Hubble sequence is shortly reviewed and discussed from the standpoint of the model. More specifically, (i) elliptical galaxies are considered as isolated systems, and an allowed region within Ellipsoidland (Hunter & de Zeeuw 1997), related to the occurrence of bifurcation points from ellipsoidal to pear-shaped configurations, is shown to be consistent with observations; (ii) elliptical galaxies are considered as embedded within dark matter haloes and, under reasonable assumptions, it is shown that tidal effects from embedding haloes have little influence on the above mentioned results; (iii) dark matter haloes and hosted elliptical galaxies, idealized as a single homeoidally striated Jacobi ellipsoid, are considered in connection with the cosmological transition from expansion to relaxation, by generalizing an earlier model (Thuan & Gott 1975), and the existence of a lower limit to the flattening of relaxed (oblate-like) configurations, is established. On the other hand, no lower limit is found to the elongation of relaxed (prolate-like) configurations, and the observed lack of elliptical galaxies more elongated than $E7$ needs a different physical interpretation, such as the occurrence of bending instabilities (Polyachenko & Shukhman 1979; Merritt & Hernquist 1991).
keywords - cosmology: dark matter - galaxies: evolution - galaxies: formation - galaxies: haloes - galaxies: structure.

1 Introduction

Large-scale celestial objects, represented as self-gravitating fluids, exhibit different features according if their subunits, or "particles", are "collisional" or "collisionless".

In the former alternative, the gravitational field that is generated by the system as a whole is negligible in respect of the force between two colliding subunits, when they repel each other strongly. Consequently, particles in self-gravitating, collisional fluids, are subjected to violent and short-lived accelerations as they are sufficiently close to each other, interspersed with longer periods when they move at nearly constant velocity.

In the latter alternative, the gravitational field that is generated by the system as a whole is dominant in respect of the force between two subunits, even if they are close to each other. Consequently, particles in self-gravitating, collisionless fluids, are subjected to smooth and long-lived accelerations through their trajectories.

Gas in stars and stars in stellar systems may be approximated, to a good extent, as collisional and collisionless, ideal self-gravitating fluids, respectively. The statistical problem of particle motion in the latter case is that of the former, with the collisions left out. "Ideal" has to be intended as "particles collide as perfectly and undeformable spheres" in the former situation, and "particles do not interact each other at all" in the latter.

The motion equation of fluid flow turns out to be the same for both collisional and collisionless fluids (e.g., Jeans 1929, Chap. II, § 26, Chap. VII, §§ 211-215; Binney & Tremaine 1987, Chap. 4, § 4.2) provided gases are thought of as far from equilibrium. Then the velocity distribution of molecules no longer obeys Maxwell distribution and is, in general, anisotropic; accordingly, the pressure is represented by a stress tensor. In the special case of isotropic velocity distributions, the pressure attains its usual meaning and the motion equation reduces to Euler's equation, provided the velocity of an infinitesimal fluid element is intended as the mean velocity of all the particles within the same element at the time considered. On the contrary, Euler's equation for a given fluid with isotropic distribution can be generalized to an anisotropic one, by replacing velocities with mean velocities and pressures with stress tensors, in the sense specified above.

For special classes of ideal, self-gravitating fluids, such as steadily rotating polytropes with polytropic index $n \geq 1/2$ (Vandervoort 1980a) and isothermal spheres (e.g., Binney & Tremaine 1987, Chap. 4, § 4.4b), a one-to-one correspondence has been discovered between collisional and collisionless systems with equal physical parameters. Steadily rotating polytropes may be represented, to a first extent, as steadily rotating, homeoidally striated ellipsoids (e.g., Vandervoort 1980b; Vandervoort & Welty 1981; Lai et al. 1993).

Though most astronomical bodies exhibit ellipsoidal-like shapes and isopycnic surfaces, still some caution must be used in dealing with the above approximation, with regard to local values of physical parameters. This is why steadily rotating polytropes are in hydrostatic equilibrium while, owing to Hamy's theorem (e.g., Chambat 1994), the contrary holds for their

homeoidally striated ellipsoidal counterparts. On the other hand, homeoidally striated ellipsoids may safely be assumed as a viable approximation to self-gravitating fluids, with regard to typical values of physical parameters, averaged over the whole volume [1](e.g., Vandervoort 1980b; Vandervoort & Welty 1981; Lai et al. 1993).

Celestial objects have been modelled as collisional, self-gravitating fluids, in particular homeoidally striated ellipsoids, since the beginning of the scientific era (see e.g., Chandrasekhar 1969, Chap. 1). The evidence of rotation in spiral galaxies and the symmetry of figure shown by elliptical galaxies and spiral bulges, suggested the following (e.g., Jeans 1929, Chap. XIII, § 299): (i) all (regular) galaxies rotate; (ii) the symmetry of figure is precisely such as rotation might be expected to produce; (iii) the observed shapes of (regular) galaxies can be explained as the figures assumed by masses rotating under their own gravitation. In particular, the system of primeval stars must have conserved roughly the same shape as the original mass of gas from which it emerged (e.g., Blaauw 1965).

The above outlined ideas were accepted up to about thirthy years ago, when observations yielded increasing evidence, that giant elliptical galaxies cannot be sustained by systematic rotation (e.g., Bertola & Capaccioli 1975; Binney 1976; Illingworth 1977, 1981; Schechter & Gunn 1979). Then giant elliptical galaxies must necessarily be conceived as collisionless, self-gravitating fluids, owing their boundaries to anisotropic peculiar velocity distribution of stars (Binney 1976, 1978), with a negligible contribution from figure rotation. Accordingly, the shape corresponds - in general - to triaxial [2]ellipsoids. Owing to high-resolution simulations, the same holds also for (nonbaryonic) dark matter haloes hosting galaxies and cluster of galaxies (e.g., Hoeft et al. 2004; Rasia et al. 2004; Bailin & Steinmetz 2004).

Isotropic peculiar velocity distributions necessarily imply configurations which rotate around the minor axis. Accordingly, empirical evidence of systematic rotation around the major axis (e.g., Bertola & Galletta 1978), in absence of tidal potential, makes a signature of the occurrence of anisotropic peculiar velocity distribution.

[1]An important exception is the energy ratio of rotational to random motions, E_{rot}/E_{pec} (Caimmi 1979, 1983).

[2]Strictly speaking, all tridimensional bodies may be conceived as triaxial, in particular spheres and spheroids. Throughout this paper, "triaxial" shall be intended as denoting ellipsoids where the axes are different in length.

Though anisotropy in peculiar velocity distribution is a basic ingredient in the description and investigation of stellar systems and hosting dark matter haloes, conceived as self-gravitating collisionless fluids (e.g., Binney 1976, 1978, 1980), still no attempt (to the knowledge of the author) has been made to gain more insight into the intrinsic connection between systematic and random motions, and the extent to which they are related in determining the figure of equilibrium. The current paper aims to overhelm the above mentioned gap, using a theory where systematic and random motions are unified.

To this aim, the effect of anisotropy in peculiar velocity distribution shall be related to the effect of systematic (real or imaginary) rotation (Caimmi 1996b). It will be shown the existence of a one-to-one correspondance between configurations characterized by systematic (*real*) rotation and *anisotropic* peculiar velocity distribution, on one hand, and configurations characterized by systematic (*real* or *imaginary*; *prograde* and/or *retrograde*) rotation and *isotropic* peculiar velocity distribution.

An alternative explanation for the absence of elliptical galaxies (and non-baryonic dark matter haloes) more flattened or elongated than $E7$ as due to bending instabilities, has been suggested long time ago from analytical considerations involving homogeneous (oblate and prolate) spheroids (Polyachenko & Shukhman 1979; Fridman & Polyachenko 1984, Vol. 1, Chap. 4, Sect. 3.3, see also pp. 313-322; Vol. 2, p. 159) and numerical simulations involving inhomogeneous (oblate and prolate) spheroids (Merritt & Hernquist 1991; Merritt & Sellwood 1994).

In a cosmological scenario (Thuan & Gott 1975), the occurrence of a limiting ellipticity in oblate configurations depends on the amount of spin growth regardless from the onset of bending instabilities. An interesting question could be if a similar conclusion holds for prolate configurations. It will be seen that the onset of bending instabilities is necessary for the occurrence of a limiting ellipticity in prolate configurations.

The current paper is organized as follows. The general theory of homeoidally striated density profiles, and the results of interest to the aim of this investigation, are outlined in Sect. 2. A unified theory of systematic and random motions, implying a definition of imaginary rotation, is developed in Sect. 3 where, in addition, an interpretation is provided to recent results from numerical simulations on stability. An application of the above mentioned theory, namely a physical interpretation of the early Hubble sequence, is performed

in Sect. 4, on general grounds, by considering (i) elliptical galaxies as isolated systems; (ii) elliptical galaxies as embedded in dark matter haloes; (iii) dark matter haloes and hosted elliptical galaxies, idealized as a single homeoidally striated Jacobi ellipsoid, in connection with the cosmological transition from expansion to relaxation; and establishing the existence of a lower limit to the flattening of relaxed (oblate-like) configurations. Some concluding remarks are drawn in Sect. 5, and a few arguments are treated with more detail in the Appendix.

2 General theory

2.1 Homeoidally striated density profiles

A general theory for homeoidally striated density profiles has been developed in earlier approaches (Roberts 1962; Caimmi 1993a; Caimmi & Marmo 2003, 2005 [3], hereafter quoted as CM03, CM05, respectively), and an interested reader is addressed therein for deeper insight. What is relevant for the current investigation, shall be mentioned and further developed here.

The isopycnic (i.e. constant density) surfaces are defined by the following law:

$$\rho = \rho_0 f(\xi) \quad ; \quad f(1) = 1 \quad ; \quad \rho_0 = \rho(1) \quad ; \tag{1a}$$

$$\xi = \frac{r}{r_0} \quad ; \quad 0 \leq \xi \leq \Xi \quad ; \quad \Xi = \frac{R}{r_0} \quad ; \tag{1b}$$

where ρ_0, r_0, are a scaling density and a scaling radius, respectively, related to a reference isopycnic surface, ξ is a scaled distance, independent of the direction along which radial coordinates are calculated, and $\Xi = \xi(r)$, is related to the boundary, where $r = R$. Both cored and cuspy density profiles, according to the explicit expression chosen for the scaled density, $f(\xi)$, are represented by Eqs. (1). In the former alternative, it is used a different normalization with respect to Caimmi (1993a), where $\xi = r/R$ and ρ_0 is the central density.

The mass, the inertia tensor, and the potential self-energy tensor are:

$$M = \nu_{mas} M_0 \quad ; \tag{2}$$

[3] A more extended version is available at the arxiv electronic site, as astro-ph/505306.

$$I_{pq} = \delta_{pq} \nu_{inr} M a_p^2 \quad ; \tag{3}$$

$$(E_{sel})_{pq} = -\frac{GM^2}{a_1} \nu_{sel} (B_{sel})_{pq} = -\frac{GM^2}{a_1} \mathcal{S}_{pq} \quad ; \tag{4}$$

$$E_{sel} = \sum_{i=1}^{3} (E_{sel})_{ii} = \frac{GM^2}{a_1} \nu_{sel} B_{sel} = -\frac{GM^2}{a_1} \mathcal{S} \quad ; \tag{5}$$

$$(B_{sel})_{pq} = \delta_{pq} \epsilon_{p2} \epsilon_{p3} A_p \quad ; \quad B_{sel} = \sum_{s=1}^{3} \epsilon_{s2} \epsilon_{s3} A_s \quad ; \tag{6}$$

$$\mathcal{S}_{pq} = \nu_{sel} (B_{sel})_{pq} \quad ; \quad \mathcal{S} = \nu_{sel} B_{sel} \quad ; \tag{7}$$

where δ_{pq} is the Kronecker symbol; G is the constant of gravitation; ν_{mas}, ν_{inr}, ν_{sel}, are profile factors i.e. depend only on the density profile via the scaled radius, Ξ; a_1, a_2, a_3, are semiaxes; $\epsilon_{pq} = a_p/a_q$ are axis ratios; A_1, A_2, A_3, are shape factors i.e. depend only on the axis ratios; and M_0 is the mass of a homogeneous ellipsoid with same density and boundary as the reference isopycnic surface:

$$M_0 = \frac{4\pi}{3} \rho_0 a_{01} a_{02} a_{03} \quad ; \tag{8}$$

where a_{01}, a_{02}, a_{03}, are the semiaxes of the ellipsoid bounded by the reference isopycnic surface.

The limiting case of homogeneous configurations reads:

$$f(\xi) = 1 \quad , \quad 0 \leq \xi \leq \Xi \quad ; \tag{9a}$$

$$\nu_{mas} = \Xi^3 \quad ; \quad \nu_{inr} = \frac{1}{5} \quad ; \quad \nu_{sel} = \frac{3}{10} \quad ; \tag{9b}$$

for further details, see CM03, CM05.

2.2 Homeoidally striated Jacobi ellipsoids

In dealing with angular momentum and rotational energy, the preservation of (triaxial) ellipsoidal shape imposes severe constraints on the rotational velocity field. Leaving an exhaustive investigation to more refined approaches, our attention shall be limited here to the special case of homeoidally striated Jacobi ellipsoids (CM05). Accordingly, the systematic velocity field is defined by the law:

$$\frac{v_{rot}(r,\theta)}{v_{rot}(R,\theta)} = \frac{v_{rot}(a'_p,0)}{v_{rot}(a_p,0)} \quad ; \tag{10}$$

or equivalently, the angular (with respect to x_3 axis) velocity field is defined by the law:

$$\frac{\Omega(r,\theta)}{\Omega(R,\theta)} = \frac{\Omega(a'_p,0)}{\Omega(a_p,0)} \quad ; \tag{11}$$

where (r,θ), (R,θ), represent a point on a generic isopycnic surface and on the boundary, respectively, along a fixed radial direction, and $(a'_p,0)$, $(a_p,0)$, $p=1,2$, represent the end of the corresponding equatorial semiaxis.

It is worth noticing that the following special cases are described by Eqs. (10) or (11): (a) rigid rotation; (b) constant rotation velocity everywhere; (c) rigid rotation of isopycnic surfaces and constant rotation velocity on the equatorial plane. To maintain ellipsoidal shapes, differential rotation [e.g., cases (b) and (c) above] must necessarily be restricted to axysimmetric figures i.e. spheroidal configurations. In the limiting situation of homogeneous, rigidly rotating, dynamical (or hydrostatic) equilibrium configurations, homeoidally striated Jacobi ellipsoids reduce to classical Jacobi ellipsoids (CM05).

The angular-momentum vector and the rotational-energy tensor are:

$$J_s = \delta_{s3}\eta_{anm}\nu_{anm}Ma_p(1+\epsilon_{qp}^2)(v_{rot})_p \quad ; \quad p\neq q\neq s \quad ; \tag{12}$$

$$(E_{rot})_{pq} = \delta_{pq}(1-\delta_{p3})\eta_{rot}\nu_{rot}M\left[(v_{rot})_p\right]^2 \quad ; \tag{13}$$

and the related module and trace, respectively, read:

$$J = \eta_{anm}\nu_{anm}M(1+\epsilon_{21}^2)a_1(v_{rot})_1 \quad ; \tag{14}$$

$$E_{rot} = \eta_{rot}\nu_{rot}M(1+\epsilon_{21}^2)\left[(v_{rot})_1\right]^2 \quad ; \tag{15}$$

where $\eta_{anm}\nu_{anm}$, η_{rot}, are shape factors, ν_{amn}, ν_{rot}, are profile factors, $(v_{rot})_p$ is the rotational velocity at the end of the semiaxis, a_p, $p=1,2$, and the rotation axis has been chosen to be x_3. For further details, see CM03, CM05.

The combination of Eqs. (14) and (15) yields:

$$(E_{rot})_{pq} = \frac{J^2}{Ma_1^2}\nu_{ram}(B_{ram})_{pq} = \frac{J^2}{Ma_1^2}\mathcal{R}_{pq} \quad ; \tag{16a}$$

$$\nu_{ram} = \frac{\nu_{rot}}{\nu_{anm}^2} \quad ; \tag{16b}$$

$$(B_{ram})_{pq} = \delta_{pq}(1-\delta_{p3})\frac{\eta_{rot}}{\eta_{anm}^2}\frac{\epsilon_{p1}^2}{(1+\epsilon_{21}^2)^2} \quad ; \tag{16c}$$

$$\mathcal{R}_{pq} = \nu_{ram}(B_{ram})_{pq} \quad ; \tag{16d}$$

which makes an alternative expression of the rotation-energy tensor, and:

$$E_{rot} = \frac{J^2}{Ma_1^2}\nu_{ram}B_{ram} = \frac{J^2}{Ma_1^2}\mathcal{R} \quad ; \tag{17a}$$

$$B_{ram} = \frac{\eta_{rot}}{\eta_{anm}^2}\frac{1}{1+\epsilon_{21}^2} \quad ; \tag{17b}$$

$$\mathcal{R} = \nu_{ram}B_{ram} \quad ; \tag{17c}$$

which makes an alternative expression of the rotation energy.

The limiting situations outlined above, read:

$$\nu_{anm} = \nu_{rot} = \nu_{inr} = \frac{1}{5} \quad ; \qquad \nu_{ram} = \nu_{inr}^{-1} = 5 \quad ; \tag{18}$$

for homogeneous configurations in rigid rotation, according to case (a);

$$\nu_{anm} = \frac{1}{4} \quad ; \qquad \nu_{rot} = \frac{1}{3} \quad ; \qquad \nu_{ram} = \frac{16}{3} \quad ; \tag{19}$$

for homogeneous configurations with constant velocity on the equatorial plane, according to cases (b) and (c);

$$\eta_{anm} = 1 \quad ; \qquad \eta_{rot} = \frac{1}{2} \quad ; \tag{20}$$

for rigidly rotating isopycnic surfaces, cases (a) and (c);

$$\eta_{anm} = \frac{3\pi}{8} \quad ; \qquad \eta_{rot} = \frac{3}{4} \quad ; \tag{21}$$

for constant velocity everywhere, case (b). Further details can be found in CM03, CM05.

2.3 Virial equilibrium configurations

The virial theorem holds for mass distributions which always remain confined within a finite region of space, and the virial equations are satisfied, with regard to values of parameters averaged over a sufficiently long time, $t \gg T$, where T is a characteristic period of the system (e.g., Landau & Lifchitz 1966, Chap. II, § 10). Let us define virial equilibrium as characterized by the

validity of the virial theorem, and relaxed and unrelaxed configurations as systems where virial equilibrium does and does not coincide, respectively, with dynamical (or hydrostatic) equilibrium (CM05).

Let us define systematic and peculiar motions as related to velocity fields where the mean value is different from or equal to zero, respectively. For instance, star motions may safely be conceived as systematic in galactic disks, and peculiar in galactic spheroids. In the formulation of the virial equations, systematic motions related to axial rotation shall explicitly be treated, and the remaining contributions (e.g., vorticity, streaming, peculiar motions) shall globally be considered together, and denoted as "residual motions". If peculiar motions may safely be thought of as dominant, apart from systematic rotation, then in the following "residual" has to be intended as "peculiar".

With regard to unrelaxed configurations, the generalized tensor virial equations read (CM05):

$$(E_{sel})_{pq} + 2(E_{rot})_{pq} + 2\zeta_{pq} E_{res} = 0 \quad ; \tag{22}$$

$$\zeta_{pq} = \frac{(\tilde{E}_{res})_{pq}}{E_{res}} \quad ; \qquad p = 1,2,3 \quad ; \qquad q = 1,2,3 \quad ; \tag{23}$$

$$\sum_{p=1}^{3} \zeta_{pp} = \frac{\tilde{E}_{res}}{E_{res}} = \zeta \quad ; \qquad 0 \leq \zeta_{pp} \leq \zeta \quad ; \tag{24}$$

$$\zeta_{pq} = 0 \quad ; \qquad p \neq q \quad ; \tag{25}$$

where ζ_{pq} is the generalized anisotropy tensor, E_{res} is the residual energy, and $(\tilde{E}_{res})_{pq} = \zeta_{pq} E_{res}$ is the effective residual-energy tensor i.e. the right amount needed for the configuration of interest to be relaxed. The diagonal components of the generalized anisotropy tensor, ζ_{pp}, may be conceived as generalized anisotropy parameters. The related trace, ζ, may be conceived as a virial index, where $\zeta = 1$ corresponds to null virial excess, $2\Delta E_{res} = 2(\tilde{E}_{res} - E_{res})$, which does not necessarily imply a relaxed configuration [4], $\zeta > 1$ to positive virial excess, and $\zeta < 1$ to negative virial excess.

Let us define the effective anisotropy tensor, as:

$$\tilde{\zeta}_{pq} = \frac{(\tilde{E}_{res})_{pq}}{\tilde{E}_{res}} \quad ; \qquad p = 1,2,3 \quad ; \qquad q = 1,2,3 \quad ; \tag{26}$$

[4]For instance, a homogeneous sphere undergoing coherent oscillations exhibits $\zeta > 1$ at expansion turnover and $\zeta < 1$ at contraction turnover. Then it necessarily exists a configuration where $\zeta = 1$ which, on the other hand, is unrelaxed.

$$\sum_{p=1}^{3} \tilde{\zeta}_{pp} = 1 \quad ; \qquad 0 \leq \tilde{\zeta}_{pp} \leq 1 \quad ; \tag{27}$$

$$\tilde{\zeta}_{pq} = 0 \quad ; \qquad p \neq q \quad ; \tag{28}$$

where the diagonal components, $\tilde{\zeta}_{pp}$, may be conceived as effective anisotropy parameters. The combination of Eqs. (23), (24), and (26) yields:

$$\tilde{\zeta}_{pp} = \frac{\zeta_{pp}}{\zeta} \quad ; \qquad p = 1, 2, 3 \quad ; \tag{29}$$

and the specification of the effective and generalized anisotropy parameters, $\tilde{\zeta}_{pp}$ and ζ_{pp}, and the residual kinetic energy, E_{res}, implies the specification of the effective, residual kinetic-energy tensor, $(\tilde{E}_{res})_{pq}$.

The substitution of Eqs. (4)-(7) and (16)-(17) into the virial equations (22), and the particularization to the rotation axis, $p = 3$, allows the following expression of the residual energy (CM05):

$$E_{res} = \frac{1}{2} \frac{GM^2}{a_1} \frac{\mathcal{S}_{33}}{\zeta_{33}} \quad ; \tag{30}$$

accordingly, the remaining virial equations read (CM05):

$$(\zeta_{33}\mathcal{S}_{qq} - \zeta_{qq}\mathcal{S}_{33}) - 2h\zeta_{33}\mathcal{R}_{qq} = 0 \quad ; \qquad q = 1, 2 \quad ; \tag{31}$$

$$h = \frac{J^2}{GM^3 a_1} \quad ; \tag{32}$$

where h may be conceived as a rotation parameter. It is apparent that Eq. (31) admits real solutions provided the following inequalities hold:

$$\frac{\zeta_{qq}}{\zeta_{33}} \leq \frac{\mathcal{S}_{qq}}{\mathcal{S}_{33}} \quad ; \qquad q = 1, 2 \quad ; \tag{33}$$

which is the natural extension of its counterpart related to axisymmetric, relaxed configurations (Wiegandt1982a,b).

2.4 Rotation and anisotropy parameters

To get a more evident connection with the centrifugal potential on the boundary, let us define the rotation parameter (CM05):

$$\upsilon = \frac{\Omega^2}{2\pi G\bar{\rho}} \quad ; \tag{34}$$

where $\Omega = \Omega(a_1, 0)$ is the angular velocity at the end of the major equatorial semiaxis, denoted as a_1, and $\bar{\rho}$ is the mean density of the ellipsoid:

$$\bar{\rho} = \frac{3}{4\pi} \frac{M}{a_1 a_2 a_3} \quad ; \tag{35}$$

the above definition of the rotation parameter, υ, makes a generalization of some special cases mentioned in the literature (e.g., Jeans 1929, Chap. IX, §232; Chandrasekhar & Leboviz 1962).

The combination of Eqs. (14), (32), (34), and (35) yields:

$$h = \frac{3}{2} \eta_{anm}^2 \nu_{anm}^2 \frac{(1+\epsilon_{21}^2)^2}{\epsilon_{21}\epsilon_{31}} \upsilon \quad ; \tag{36}$$

which links the rotation parameters, h and υ. An explicit expression of the rotation parameter, h, may directly be obtained from Eq. (31), as:

$$h = \frac{1}{2} \frac{\zeta_{33}\mathcal{S}_{qq} - \zeta_{qq}\mathcal{S}_{33}}{\zeta_{33}\mathcal{R}_{qq}} \quad ; \quad q = 1, 2 \quad ; \tag{37}$$

and the substitution of Eqs. (37) into (36), using (16) and (17), allows the explicit expression of the rotation parameter, υ, as:

$$\upsilon = \frac{1}{3} \frac{\epsilon_{21}\epsilon_{31}}{(1+\epsilon_{21}^2)^2} \frac{1}{\eta_{amn}^2 \nu_{amn}^2} \frac{\zeta_{33}\mathcal{S}_{qq} - \zeta_{qq}\mathcal{S}_{33}}{\zeta_{33}\mathcal{R}_{qq}} \quad ; \quad q = 1, 2 \quad ; \tag{38}$$

which, in the special case of rigidly rotating, homogeneous configurations with isotropic peculiar velocity distribution, reduces to a known relation for Jacobi ellipsoids and, with the additional demand of axial symmetry, to a known relation for MacLaurin spheroids (e.g., Jeans 1929, Chap. VIII, §§189-193; Chandrasekhar 1969, Chap. 5, §32, Chap. 6, §39; Caimmi 1996a).

An explicit expression of anisotropy parameter ratio, can be obtained via Eq. (37). The result is (CM05):

$$\frac{\zeta_{qq}}{\zeta_{33}} = \frac{\mathcal{S}_{qq}}{\mathcal{S}_{33}} \left[1 - 2h \frac{\mathcal{R}_{qq}}{\mathcal{S}_{qq}} \right] \quad ; \quad q = 1, 2 \quad ; \tag{39}$$

$$\frac{\zeta_{11}}{\zeta_{22}} = \frac{\mathcal{S}_{11} - 2h\mathcal{R}_{11}}{\mathcal{S}_{22} - 2h\mathcal{R}_{22}} \quad ; \tag{40}$$

and the combination of Eqs. (24) and (39) yields:

$$\frac{\zeta_{33}}{\zeta} = \frac{\mathcal{S}_{33}}{\mathcal{S} - 2h\mathcal{R}} \quad ; \tag{41}$$

which provides an alternative expression to Eqs. (37) and (38), as:

$$h = \frac{1}{2}\frac{\zeta_{33}\mathcal{S} - \zeta\mathcal{S}_{33}}{\zeta_{33}\mathcal{R}} \quad ; \tag{42}$$

$$\upsilon = \frac{1}{3}\frac{\epsilon_{21}\epsilon_{31}}{(1+\epsilon_{21}^2)^2}\frac{1}{\eta_{amn}^2\nu_{amn}^2}\frac{\zeta_{33}\mathcal{S} - \zeta\mathcal{S}_{33}}{\zeta_{33}\mathcal{R}} \quad ; \tag{43}$$

that are equivalent to Eq. (31), and then admit real solutions provided inequality (33) is satisfied.

Finally, Eqs. (31) may be combined as:

$$\frac{\mathcal{R}_{11}}{\mathcal{R}_{22}} = \frac{\zeta_{33}\mathcal{S}_{11} - \zeta_{11}\mathcal{S}_{33}}{\zeta_{33}\mathcal{S}_{22} - \zeta_{22}\mathcal{S}_{33}} \quad ; \tag{44}$$

where it can be seen that Eqs. (40) and (44) are changed one into the other, by replacing the terms, $\mathcal{S}_{33}\zeta_{qq}/\zeta_{33}$, with the terms, $2h\mathcal{R}_{qq}$, and vice versa. The above results may be reduced to a single statement.

Theorem 1. *Given a homeoidally striated Jacobi ellipsoid, rotating around an axis, x_3, the relation:*

$$\frac{X_{11}}{X_{22}} = \frac{\mathcal{S}_{11} - Y_{11}}{\mathcal{S}_{22} - Y_{22}} \quad ;$$

$$X_{qq} = \frac{\zeta_{qq}}{\zeta_{33}}\mathcal{S}_{33} \quad , \quad 2h\mathcal{R}_{qq} \quad ; \qquad q = 1, 2 \quad ;$$

$$Y_{qq} = 2h\mathcal{R}_{qq} \quad , \quad \frac{\zeta_{qq}}{\zeta_{33}}\mathcal{S}_{33} \quad ; \qquad q = 1, 2 \quad ;$$

is symmetric with respect to X_{qq} and Y_{qq}, being the former tensor related to anisotropic residual velocity distribution, and the latter one to systematic rotation around the axis, x_3, or vice versa.

In the special case of axisymmetric configurations, the shape factors related to equatorial axes coincide, $A_2 = A_1$, as $\epsilon_{21} = 1$ (e.g., CM05). Then

$\mathcal{S}_{11} = \mathcal{S}_{22}$ owing to Eqs. (6), (7), and $\mathcal{R}_{11} = \mathcal{R}_{22}$ owing to Eqs. (17), which necessarily imply $\zeta_{11} = \zeta_{22}$, owing to Eq. (44).

In the general case of triaxial configurations, the contrary holds, $A_2 \neq A_1$, as $\epsilon_{21} \neq 1$, then $\mathcal{S}_{11} \neq \mathcal{S}_{22}$ and $\mathcal{R}_{11} \neq \mathcal{R}_{22}$, then the equality, $\zeta_{11} = \zeta_{22}$, via Eq. (40), implies the validity of the relation:

$$h = \frac{1}{2}\frac{\mathcal{S}_{11} - \mathcal{S}_{22}}{\mathcal{R}_{11} - \mathcal{R}_{22}} \quad ; \tag{45}$$

if otherwise, the residual velocity distribution along the equatorial plane [5] is anisotropic i.e. $\zeta_{11} \neq \zeta_{22}$. The related degeneracy can be removed using an additional condition, as it will be shown in the next section.

The above results may be reduced to a single statement.

Theorem 2. *Isotropic residual velocity distribution along the equatorial plane, $\zeta_{11} = \zeta_{22}$, makes a necessary condition for homeoidally striated Jacobi ellipsoids to be symmetric with respect to the rotation axis, x_3, i.e. reduce to homeoidally striated MacLaurin spheroids.*

3 A unified theory of systematic and random motions

3.1 Imaginary rotation

A unified theory of systematic and random motions is allowed, taking into consideration imaginary rotation. It has been shown above that Eq. (31), or equivalently one among (37), (38), (42), (43), admits real solutions provided inequality (33) is satisfied. If otherwise, the rotation parameter - let it be h or υ - has necessarily to be negative, which implies, via Eqs. (32) or (34), an *imaginary* angular velocity, $\mathrm{i}\Omega$, where i is the imaginary unit. Accordingly, the centrifugal potential takes the general expression:

$$\mathcal{T}^{\mp}(x_1, x_2, x_3) = \mp\frac{1}{2}[\Omega(x_1, x_2, x_3)]^2 w^2 \quad ; \qquad w^2 = x_1^2 + x_2^2 \quad ; \tag{46}$$

[5] Throughout this paper, "along the equatorial plane" has to be intended as "along any direction parallel to the equatorial plane".

where the minus and the plus correspond to imaginary and real rotation, respectively. The centrifugal force related to real rotation, $\partial\mathcal{T}^{+}/\partial w$, has opposite sign with respect to the gravitational force, $\partial\mathcal{V}/\partial w$. On the other hand, the centrifugal force related to imaginary rotation, $\partial\mathcal{T}^{-}/\partial w$, has equal sign with respect to the gravitational force, $\partial\mathcal{V}/\partial w$. Then the net effect of real rotation is flattening, while the net effect of imaginary rotation is *elongation*, with respect to the rotation axis (Caimmi 1996b).

To get further insight, let us particularize Eq. (31) to the special case of null rotation ($h = 0$). The result is:

$$\frac{\zeta_{qq}}{\zeta_{33}} = \frac{\mathcal{S}_{qq}}{\mathcal{S}_{33}} \quad ; \qquad h = 0 \quad ; \qquad q = 1, 2 \quad ; \tag{47}$$

where the right-hand side, via Eqs. (6) and (7), depends on the axis ratios only. It can be seen (Appendix A) that $\mathcal{S}_{qq}/\mathcal{S}_{33} \geq 1$ for oblate-like configurations ($a_1 \geq a_2 \geq a_3$), and $\mathcal{S}_{qq}/\mathcal{S}_{33} \leq 1$ for prolate-like configurations ($a_2 \leq a_1 \leq a_3$), which implies $\zeta_{qq}/\zeta_{33} \geq 1$ for oblate-like configurations, and $\zeta_{qq}/\zeta_{33} \leq 1$ for prolate-like configurations. Accordingly, the net effect of positive or negative residual motion excess along the equatorial plane is flattening or elongation, respectively. In what follows, it shall be intended that residual motion excess is related to the equatorial plane.

The above considerations show a strict connection between real rotation and positive residual motion excess, on one hand, and between imaginary rotation and negative residual motion excess, on the other hand. At this point, it is natural to ask if (positive or negative) residual motion excess can be interpreted as (real or imaginary) rotation, and vice versa.

3.2 Residual motion excess and rotation

With regard to the rotation parameter, υ, it is convenient to use the more compact notation [6]:

$$\upsilon_N = \frac{3\eta_{rot}\nu_{rot}}{\nu_{sel}}\upsilon \quad ; \tag{48}$$

and the substitution of Eqs. (6), (7), (16), (17), (29), into (38) and (43), yields the equivalent expressions:

$$\upsilon_N = A_q - \frac{\zeta_{qq}}{\zeta_{33}}\epsilon_{3q}^2 A_3 \quad ; \qquad q = 1, 2 \quad ; \tag{49}$$

[6] The factor, 3, does not appear in CM05: $\upsilon_N = 3(\upsilon_N)_{CM05}$.

$$\upsilon_N = \frac{1}{1+\epsilon_{21}^2}\left[A_1 + \epsilon_{21}^2 A_2 + \frac{\zeta_{33}-\zeta}{\zeta_{33}}\epsilon_{31}^2 A_3\right] \quad ; \tag{50}$$

which shows that, for homeoidally striated Jacobi ellipsoids, the normalized rotation parameter, υ_N, depends on the axis ratios, ϵ_{21}, ϵ_{31}, and a *single* anisotropy parameter, $\tilde{\zeta}_{33} = \zeta_{33}/\zeta$. In the special case of homogeneous, rigidly rotating configurations, owing to Eqs. (9b), (18), and (20), Eq. (48) reduces to: $\upsilon_N = \upsilon$.

In the limit of isotropic residual velocity distribution, $\zeta_{11} = \zeta_{22} = \zeta_{33} = \zeta/3$, Eqs. (49) and (50) take the simpler form:

$$(\upsilon_N)_{iso} = A_q - \epsilon_{3q}^2 A_3 \quad ; \qquad q = 1, 2 \quad ; \tag{51}$$

$$(\upsilon_N)_{iso} = \frac{1}{1+\epsilon_{21}^2}\left[A_1 + \epsilon_{21}^2 A_2 - 2\epsilon_{31}^2 A_3\right] \quad ; \tag{52}$$

where the index, *iso*, means isotropic residual velocity distribution.

Accordingly, Eqs. (49) and (50) may be expressed as:

$$\upsilon_N = (\upsilon_N)_{iso} - (\upsilon_N)_{ani} \quad ; \tag{53}$$

$$(\upsilon_N)_{ani} = \left(\frac{\zeta_{qq}}{\zeta_{33}} - 1\right)\epsilon_{3q}^2 A_3 \quad ; \tag{54}$$

$$(\upsilon_N)_{ani} = \left(\frac{\zeta}{\zeta_{33}} - 3\right)\frac{\epsilon_{31}^2 A_3}{1+\epsilon_{21}^2} \quad ; \tag{55}$$

where $(\upsilon_N)_{ani} \geq 0$ for oblate-like configurations, $\zeta_{qq}/\zeta_{33} \geq 1$; $(\upsilon_N)_{ani} \leq 0$ for prolate-like configurations, $\zeta_{qq}/\zeta_{33} \leq 1$; and the index, *ani*, means contribution from residual motion excess. Accordingly, positive residual motion excess along the equatorial plane is related to real rotation. On the contrary, negative residual motion excess along the rotation axis is related to imaginary rotation.

Let us rewrite Eq. (53) as:

$$(\upsilon_N)_{iso} = \upsilon_N + (\upsilon_N)_{ani} \quad ; \tag{56}$$

which, owing to Eqs. (34) and (48), is equivalent to:

$$\Omega_{iso}^2 = \Omega^2 \mp \Omega_{ani}^2 \quad ; \tag{57}$$

where the plus corresponds to real rotation, $(\upsilon_N)_{ani} \geq 0$, and the minus to imaginary rotation, $(\upsilon_N)_{ani} \leq 0$. Then the effect of residual motion excess on the shape of the system, is virtually indistinguishible from the effect of additional systematic rotation, with similar (rotation) velocity distribution as the pre-existing one. The related, explicit expression, according to Eqs. (11), (34), and (55), is:

$$\frac{\Omega_{ani}(r,\theta)}{\Omega_{ani}(R,\theta)} = \frac{\Omega_{ani}(a_1',0)}{\Omega_{ani}(a_1',0)} = \frac{\Omega(a_1',0)}{\Omega(a_1',0)} = \frac{\Omega(r,\theta)}{\Omega(R,\theta)} \quad ; \tag{58}$$

$$\Omega_{ani}^2 = \Omega_{ani}^2(a_1) = \mp(\upsilon_N)_{ani} 2\pi G\overline{\rho} \quad ; \tag{59}$$

where the double sign ensures a non negative value on the right hand-side member of Eq. (59). The above results may be reduced to a single statement.

Theorem 3. *Given a homeoidally striated Jacobi ellipsoid, the effect of (positive or negative) residual motion excess is equivalent to an additional (real or imaginary) rotation, with equal spatial distribution as the pre-existing rotation, but value at the end of major equatorial axis conform to the relation:*

$$\mp\Omega_{ani}^2 = \mp\Omega_{ani}^2(a_1) = 2\pi G\overline{\rho}\left(\frac{\zeta}{\zeta_{33}} - 3\right)\frac{\epsilon_{31}^2 A_3}{1+\epsilon_{21}^2} \quad ; \tag{60}$$

with regard to an adjoint configuration where the residual velocity distribution is isotropic.

Accordingly, a homeoidally striated Jacobi ellipsoid with assigned systematic rotation and residual velocity distribution, with regard to the shape, is virtually indistinguishable from an adjoint configuration of equal mass and axes, systematic rotation velocity distribution deduced from Eqs. (11), (58) and (59), and isotropic residual velocity distribution.

Owing to Eqs. (53), (54), and (55), Eqs. (51) and (52) are equivalent to (49) and (50), respectively. On the other hand, Eqs. (51) and (52) are valid for classical Jacobi ellipsoids with rotation parameter, $\upsilon = (\upsilon_N)_{iso}$. The above results may be reduced to a single statement.

Theorem 4. *Given a homeoidally striated Jacobi ellipsoid, the adjoint configuration, characterized by isotropic residual velocity distribution and normalized rotation parameter, $(\upsilon_N)_{iso}$, exhibits same shape as a classical Jacobi ellipsoid of equal mass and axes, and rotation parameter, $\upsilon = (\upsilon_N)_{iso}$.*

Accordingly, a homeoidally striated Jacobi ellipsoid (in general, an unrelaxed configuration) with assigned systematic rotation and residual velocity distribution, with regard to the shape, is virtually indistinguishable from an adjoint, classical Jacobi ellipsoid (a relaxed configuration) of equal mass and axes, and rotation parameter equal to the normalized rotation parameter of the original configuration.

3.3 Axis ratios and anisotropy parameters

The combination of alternative expressions of the rotation parameter, $(\upsilon_N)_{iso}$, expressed by Eqs. (51), yields:

$$\epsilon_{21}^2 (A_2 - A_1) = (1 - \epsilon_{21}^2) \epsilon_{31}^2 A_3 \quad ; \tag{61}$$

which, for axisymmetric configurations, reduces to an indeterminate form, $0 = 0$.

The combination of alternative expressions of the rotation parameter, $(\upsilon_N)_{ani}$, expressed by Eqs. (54), yields:

$$\zeta_{33} - \zeta_{22} = \epsilon_{21}^2 (\zeta_{33} - \zeta_{11}) \quad ; \tag{62}$$

which, for isotropic residual velocity distributions, reduces to an indeterminate form, $0 = 0$. In addition, axisymmetric configurations ($\epsilon_{21} = 1$) necessarily imply isotropic residual velocity distributions along the equatorial plane, $\zeta_{11} = \zeta_{22}$.

The combination of Eqs. (24) and (62) yields:

$$\zeta_{11} = \frac{\zeta - (2 - \epsilon_{21}^2) \zeta_{33}}{1 + \epsilon_{21}^2} \quad ; \tag{63a}$$

$$\zeta_{22} = \frac{\epsilon_{21}^2 \zeta + (1 - 2\epsilon_{21}^2) \zeta_{33}}{1 + \epsilon_{21}^2} \quad ; \tag{63b}$$

which, for axisymmetric configurations ($\epsilon_{21} = 1$) reduces to $\zeta_{11} = \zeta_{22} = (\zeta - \zeta_{33})/2$, and the special case, $\zeta_{33} = \zeta/3$, reads $\zeta_{11} = \zeta_{22} = \zeta/3$.

The conditions, $\zeta_{11} \geq 0$, related to Eqs. (23) and (24), and $0 \leq \epsilon_{21} \leq 1$, necessarily imply $0 \leq \zeta_{33}/\zeta \leq 1/2$. If otherwise, sequences of virial equilibrium configurations cannot attain the oblong shape, $\epsilon_{21} = \epsilon_{31} = 0$, but must stop earlier, where the equivalent relations:

$$\epsilon_{21}^2 = \frac{2\zeta_{33} - \zeta}{\zeta_{33}} \quad ; \qquad \zeta_{11} = 0 \quad ; \tag{64}$$

are satisfied. The above results may be reduced to the following statements.

Theorem 5. *Given a homeoidally striated Jacobi ellipsoid, the anisotropy parameters along the equatorial plane depend on the equatorial axis ratio for triaxial configurations. The related expressions coincide, $\zeta_{11} = \zeta_{22}$, in the limit of axisymmetric configurations, $\epsilon_{21} = 1$.*

Theorem 6. *A necessary and sufficient condition for a homeoidally striated Jacobi ellipsoid to have isotropic residual velocity distribution, is that the anisotropy parameter along the rotation axis, equals one third.*

Theorem 7. *Given a sequence of homeoidally striated Jacobi ellipsoids, the ending point occurs when the equatorial axis ratio is null, $\epsilon_{31} = 0$, and/or the generalized anisotropy parameter related to the major axis is null, $\zeta_{11} = 0$, which is equivalent to $\epsilon_{21} = (2 - \zeta/\zeta_{33})^{1/2}$. The special case of dynamical (or hydrostatic) equilibrium, $\zeta = 1$, implies centrifugal support along the major axis provided $\zeta_{11} = 0$.*

Accordingly, with regard to homeoidally striated Jacobi ellipsoids, the anisotropy parameters along the equatorial plane, ζ_{11} and ζ_{22}, cannot be arbitrarily assigned, but depend on the equatorial axis ratio, ϵ_{21}, conform to Eqs. (63). On the other hand, the further knowledge of the meridional axis ratio, ϵ_{31}, and the rotation parameter, υ_N, allows the determination of the rotation parameter, $(\upsilon_N)_{ani}$, via Eqs. (51), (52), (53), and then the ratios, ζ_{qq}/ζ_{33}, ζ_{33}/ζ, via Eqs. (54), (55), respectively, or the anisotropy parameter along the rotation axis, ζ_{33}, provided the virial index, ζ, defined by Eq. (24), is assigned.

In conclusion, with regard to homeoidally striated Jacobi ellipsoids defined by assigned axis ratios, ϵ_{31}, ϵ_{21}, rotation parameter, υ_N, and virial index, ζ, the anisotropy parameters, ζ_{11}, ζ_{22}, ζ_{33}, cannot arbitrarily be fixed, but must be determined as shown above.

3.4 Sequences of virial equilibrium configurations

With regard to homeoidally striated Jacobi ellipsoids, it has been shown above that adjoints configurations are characterized by (i) centrifugal potential, $\mathcal{T}_{iso}(x_1, x_2, x_3) = \mathcal{T}(x_1, x_2, x_3) + \mathcal{T}_{ani}(x_1, x_2, x_3)$, or $\Omega^2_{iso}(x_1, x_2, x_3) =$

$\Omega^2(x_1, x_2, x_3) \mp \Omega^2_{ani}(x_1, x_2, x_3)$, where the angular velocity distribution related to residual motion excess, is defined by Eqs. (58) and (60); and (ii) isotropic residual velocity distribution. Owing to Theorem 3, a sequence of homeoidally striated Jacobi ellipsoids in virial equilibrium coincides with the sequence of adjoints configurations. The last, in turn, owing to Theorem 4, coincides with the sequence of classical Jacobi ellipsoids provided the related rotation parameters coincide, $\upsilon = (\upsilon_N)_{iso}$, conform to Eqs. (51), (52), and imaginary rotation is also considered. Given a homeoidally striated Jacobi ellipsoid with fixed axis ratios, ϵ_{21}, ϵ_{31}, rotation parameter, $(\upsilon_N)_{ani}$, and virial index, ζ, the anisotropy parameters, ζ_{11}, ζ_{22}, ζ_{33}, are determined via Eqs. (51)-(55) and (63). Negative values of the rotation parameter, $(\upsilon_N)_{iso}$, extend the sequence of classical MacLaurin spheroids to imaginary rotation i.e. prolate configurations where the major axis coincides with the rotation axis.

Once more owing to Theorem 4, the bifurcation point of a sequence of homeoidally striated Jacobi ellipsoids in virial equilibrium coincides with its counterpart along the sequence of classical Jacobi ellipsoids, $[\epsilon_{31}, (\upsilon_N)_{iso}] = (0.582724, 0.187115)$ (e.g., Jeans 1929, Chap. VIII, § 192; Chandrasekhar 1969, Chap. 5, § 33). Accordingly, the axis ratio of the configuration where the bifurcation occurs, is a solution of the transcendental equation (Caimmi 1996a):

$$\frac{\epsilon_{31}^2 A_3}{A_1} = \frac{3 - 2\epsilon_{31}^2}{5 - 4\epsilon_{31}^2} \quad ; \qquad \epsilon_{21} = 1 \quad ; \tag{65}$$

where, owing to Eqs. (118):

$$\frac{\epsilon_{31}^2 A_3}{A_1} \leq 1 \quad ; \qquad \epsilon_{31} \leq 1 \quad ; \tag{66a}$$

$$\frac{\epsilon_{31}^2 A_3}{A_1} \geq 1 \quad ; \qquad \epsilon_{31} \geq 1 \quad ; \tag{66b}$$

and further analysis of Eq. (65) shows that two solutions exist. One is related to spherical configurations ($\epsilon_{31} = \epsilon_{21} = 1$), which belong to the axisymmetric sequence ($a_1 = a_2 \neq a_3$); for this reason, it makes a parasite solution to the problem under discussion. On the contrary, the remaining solution defines the axisymmetric configuration where bifurcation takes place.

Sequences of homeoidally striated Jacobi ellipsoids can be deduced from Figs. 1 and 2. The sequence of classical MacLaurin spheroids (including

Jacobi ellipsoids), extended to the case of imaginary rotation, is shown in Fig. 1. The rotation parameter, $(\upsilon_N)_{ani}$, is plotted in Fig. 2 as a function of the axis ratio, ϵ_{31}, for different values of the effective anisotropy parameter, $\tilde{\zeta}_{33} = \zeta_{33}/\zeta$, labelled on each curve. With regard to a fixed anisotropy parameter, $\tilde{\zeta}_{33}$, the related sequence starts from a non rotating configuration, $\upsilon_N = 0$ i.e. $(\upsilon_N)_{ani} = (\upsilon_N)_{iso}$, and ends at a configuration where either $\epsilon_{31} = 0$ or $\tilde{\zeta}_{11} = 0$. The locus of the ending points related to the latter alternative, is represented as a long-dashed curve. The sequence cannot be continued on the right, as imaginary rotation i.e. larger $\tilde{\zeta}_{33}$ would be needed and a different sequence should be considered. The effect of positive ($\tilde{\zeta}_{33} < 1/3$) or negative ($\tilde{\zeta}_{33} > 1/3$) residual motion excess is equivalent to an additional real or imaginary rotation, respectively. The horizontal non negative semiaxis, $\epsilon_{31} \geq 0$, $(\upsilon_N)_{ani} = 0$, is the locus of configurations with isotropic residual velocity distribution, $\tilde{\zeta}_{33} = 1/3$. The vertical straight line, $\epsilon_{31} = 1$, is the locus of spherical configurations.

With regard to real rotation, the ending point of a sequence occurs at either null meridional axis ratio, $\epsilon_{31} = 0$, and/or null effective anisotropy parameter related to major equatorial axis direction, $\tilde{\zeta}_{11} = 0$. The occurrence of the latter situation is marked by a square on the corresponding sequence plotted in Fig. 2, and the related locus is represented as a long-dashed curve. Configurations on the left are forbidden, as they would imply negative residual energy tensor component, $(E_{res})_{11} < 0$, to satisfy the virial equation (22), which would imply imaginary rotation around major equatorial axis i.e. systematic motions other than rotation around the minor axis.

With regard to imaginary rotation, no ending point occurs and the system is allowed to attain negative infinite rotation parameter, $(\upsilon_N)_{iso} \to -\infty$, and infinite meridional axis ratio, $\epsilon_{31} \to +\infty$. The related configuration is either a spindle ($a_1 = a_2 = 0$) or an infinitely high cylinder ($a_1 = a_2 < a_3 \to +\infty$).

Further inspection to Fig. 2 shows additional features, namely: (i) null left first derivatives on each sequence at bifurcation point (not marked therein for sake of clarity), and (ii) occurrence of symmetric sequences with respect to the horizontal axis (including also forbidden configurations).

The existence of null left first derivatives on each sequence, at bifurcation point, cannot be deduced analytically but, on the other hand, it may be inferred both numerically and graphycally. Further support to this idea comes from the following considerations. Sequences branching from the bifurcation point on the left, such as those plotted in Fig. 2, are related to triaxial config-

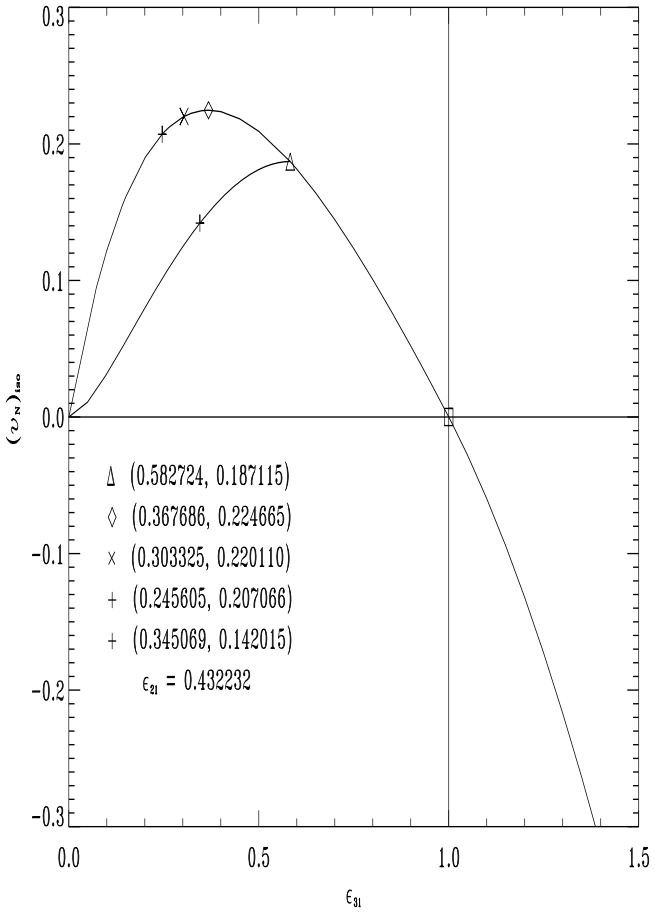

Figure 1: The sequence of classical MacLaurin spheroids, from the starting point (square) to the bifurcation point (triangle), and classical Jacobi ellipsoids, from the starting point (triangle) to the bifurcation point (lower latin cross), extended to the case of imaginary rotation (negative values of the rotation parameter, υ, which equals the normalized rotation parameter, $(\upsilon_N)_{iso}$, related to homeoidally striated Jacobi ellipsoids). Both sequences are continued in the region of instability. With regard to MacLaurin spheroids, it is also marked: the extremum point of maximum (diamond); the point at the onset of dynamical instability (St. Andreas cross); and the point at the onset of instability towards pear-shaped configurations (upper latin cross), which has its counterpart on the Jacobi sequence. Numerical values are taken from Chandrasekhar (1969, Chap. 5, §§ 32-33; Chap. 6, §§39-41). The horizontal line, $(\upsilon_N)_{iso} = 0$, $\epsilon_{31} > 0$, is the locus of non rotating configurations. The vertical line, $\epsilon_{31} = 1$, is the locus of spherical configurations. The above mentioned lines divide the non negative semiplane, $\epsilon_{31} \geq 0$, into four regions (from top left in clockwise sense): A - oblate-like shapes with real rotation; B - prolate-like shapes with real rotation; C - prolate-like shapes with imaginary rotation; D - oblate-like shapes with imaginary rotation. Regions B and D are forbidden to sequences of homeoidally striated Jacobi ellipsoids.

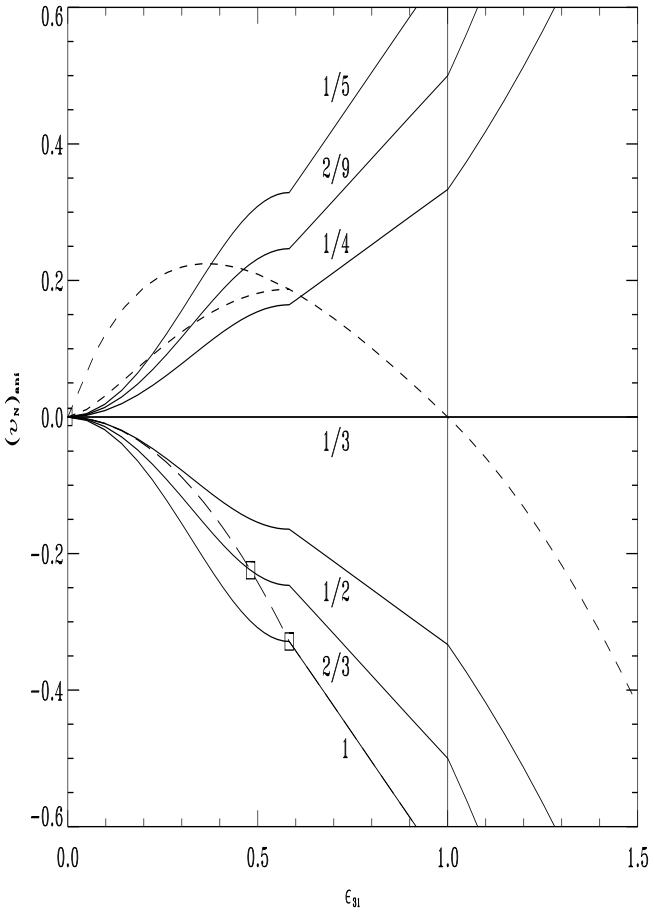

Figure 2: The normalized rotation parameter, $(\upsilon_N)_{ani}$, related to residual motion excess, as a function of the axis ratio, ϵ_{31}, with regard to homeoidally striated Jacobi ellipsoids. Each curve is labelled by the value of the generalized anisotropy parameter, $\tilde{\zeta}_{33} = \zeta_{33}/\zeta$. The horizontal non negative semiaxis, $\epsilon_{31} \geq 0$, $(\upsilon_N)_{ani} = 0$, is the locus of configurations with isotropic residual velocity distribution, $\tilde{\zeta}_{33} = 1/3$. The vertical straight line, $\epsilon_{31} = 1$, is the locus of spherical configurations. The generic sequence starts from a non rotating configuration (short-dashed curves) and ends at a configuration where either $\epsilon_{31} = 0$ or $\tilde{\zeta}_{33} = 0$ (long-dashed curve). The regions above the upper short-dashed curve and below the long-dashed curve, respectively, are forbidden. The non negative vertical semiaxis, $(\upsilon_N)_{ani} \geq 0$, $\epsilon_{31} = 0$, corresponds to flat ($\tilde{\zeta}_{33} = 0$) or oblong ($\tilde{\zeta}_{33} = \tilde{\zeta}_{22} = 0$) configurations. The curves are symmetric with respect to the horizontal axis, until the limiting curve, $\tilde{\zeta}_{33} = \tilde{\zeta} = 1$, is reached in region (D). The limiting configuration where $\tilde{\zeta}_{11} = 0$, is marked by a square: no configuration in virial equilibrium is allowed on the left, as it would imply $\tilde{\zeta}_{11} < 0$. No configuration is allowed on the right of the starting point, as it would imply $\upsilon_N < 0$. The sequence starting from the bifurcation point (not shown) corresponds to $\tilde{\zeta}_{33} = 0.241648$, $\tilde{\zeta}_{11} = \tilde{\zeta}_{22} = 0.379176$.

urations where the equatorial axis ratio does not exceed unity, $\epsilon_{21} \leq 1$. The above mentioned sequence can also be extended to adjoint configurations where $\epsilon_{21} \to 1$, $\epsilon_{21} \geq 1$, which corresponds to replacing each equatorial axis with the other. Accordingly, the extended sequence of triaxial configurations is symmetric with respect to the axis, $\epsilon_{31} = (\epsilon_{31})_{bif}$ i.e. the value related to the bifurcation point, which implies the occurrence of an extremum point of maximum or minimum, and then a null first derivative. The above results may be reduced to a single statement.

Theorem 8. *Given a sequence of homeoidally striated Jacobi ellipsoids, the contribution of residual motion excess,* $(\upsilon_N)_{ani}$*, to the rotation parameter,* $(\upsilon_N)_{iso}$*, has a null left first derivative at the bifurcation point,* $[\,\mathrm{d}(\upsilon_N)_{ani}/\,\mathrm{d}\epsilon_{31}]_{(\epsilon_{31})^-_{bif}} = 0$.

The occurrence of symmetric sequences with respect to the horizontal axis, is deduced from Eq. (55) using the condition:

$$(\tilde{\zeta}^+_{33})^{-1} - 3 = -(\tilde{\zeta}^-_{33})^{-1} + 3 \quad ; \tag{67}$$

where $\tilde{\zeta}^{\mp}_{33} = \zeta^{\mp}_{33}/\zeta$ is related to curves characterized by negative ($\tilde{\zeta}_{33} = \tilde{\zeta}^-_{33} \geq 1/3$) and positive ($\tilde{\zeta}_{33} = \tilde{\zeta}^+_{33} \leq 1/3$) values, respectively, of the rotation parameter, $(\upsilon_N)_{ani}$, see Fig. 2. Couples of symmetric sequences start from $(\tilde{\zeta}^-_{33}, \tilde{\zeta}^+_{33}) = (1/3, 1/3)$, where each curve coincides with the other, and end at (1,1/5). Sequences in the range, $0 \leq \tilde{\zeta}^+_{33} < 1/5$, have no symmetric counterpart.

Let a point, $\mathsf{P}[\epsilon_{31}, (\upsilon_N)_{iso}]$, be fixed on the extended sequence of classical Jacobi ellipsoids, and the axis ratio, ϵ_{21}, be determined by use of Eqs. (51), (52). Let a point, $\mathsf{P}'[\epsilon_{31}, (\upsilon_N)_{ani}]$, be fixed on the plane, $[\mathsf{O}\epsilon_{31}(\upsilon_N)_{ani}]$, and the generalized anisotropy parameters, $\tilde{\zeta}_{11}$, $\tilde{\zeta}_{22}$, $\tilde{\zeta}_{33}$, be determined by use of Eqs. (54), (55), (63). Finally, let the normalized rotation parameter, υ_N, be determined by use of Eq. (53). Following the above procedure, sequences of homeoidally striated Jacobi ellipsoids may be generated. For assigned density profiles and systematic rotation velocity fields, there are three independent parameters, which may be chosen as two axis ratios, ϵ_{21}, ϵ_{31}, and one generalized anisotropy parameter, $\tilde{\zeta}_{33}$.

3.5 Centrifugal support along the major equatorial axis

The calculation of the gravitational force, induced by homeoidally striated Jacobi ellipsoids, involves numerical integrations (e.g., Chandrasekhar 1969, Chap. 3, § 20) and is outside the aim of the current paper. With regard to an assigned isopycnic surface internal to, or coinciding with, the boundary, the gravitational force, F_G, induced at the end of the related major equatorial semiaxis, a'_1, satisfies the inequality:

$$[F_G(a'_1, 0, 0)]_{sph} \leq F_G(a'_1, 0, 0) \leq [F_G(a'_1, 0, 0)]_{foc} \quad ;$$

where the left-hand side is related to spherical isopycnics with unchanged major equatorial axes, and the right-hand side to confocal isopycnic surfaces from the one under consideration to the centre. Owing to Newton's and MacLaurin's theorem (e.g., Caimmi 2003), the following relations hold:

$$F_G(a'_1, 0, 0) = -2\pi G \bar{\rho}_w(a'_1)(A_1)_w a'_1 \quad ; \tag{68}$$

where $\bar{\rho}(a'_1)$ is the mean density within the isopycnic surface, and $w = sph, foc$, for the striated sphere and the focaloidally striated ellipsoid surrounded by the homeoidally striated corona, respectively.

The balance between gravitational and centrifugal force at the end of the major equatorial axis of the isopycnic surface under discussion, reads:

$$-2\pi G \bar{\rho}_w(a'_1)(A_1)_w a'_1 + \Omega^2_{iso}(a'_1) a'_1 = 0 \quad ; \tag{69}$$

where the angular velocity, Ω_{iso}, takes into account both systematic rotation and residual motion excess, according to Eq. (57). On the other hand, the generalization of Eq. (34) to a generic isopycnic surface within the boundary, reads:

$$\upsilon(a'_1) = \frac{\Omega^2(a'_1)}{2\pi G \bar{\rho}_w(a'_1)} \quad ; \tag{70}$$

and the combination of Eqs. (48), (56), (57), (69), (70), yields:

$$\{[\upsilon_{iso}(a'_1)]_{eq}\}_w = \frac{\Omega^2_{iso}(a'_1)}{2\pi G \bar{\rho}_w(a'_1)} = (A_1)_w \quad ; \tag{71}$$

where the index, eq, denotes the rotation parameter, $\upsilon_{iso}(a'_1)$, related to centrifugal support at the end of major equatorial axis of the isopycnic surface under consideration. The above results allow the validity of the relation:

$$\{[\upsilon_{iso}(a'_1)]_{eq}\}_{cof} \leq [\upsilon_{iso}(a'_1)]_{eq} \leq \{[\upsilon_{iso}(a'_1)]_{eq}\}_{sph} \quad ; \tag{72}$$

where $[\upsilon_{iso}(a_1')]_{eq}$ is the critical value related to the homeoidally striated Jacobi ellipsoid, with regard to an assigned isopycnic surface internal to, or coinciding with, the boundary. Then $\upsilon_{iso}(a_1') \geq \{[\upsilon_{iso}(a_1')]_{eq}\}_{cof}$ and $\upsilon_{iso}(a_1') \leq \{[\upsilon_{iso}(a_1')]_{eq}\}_{sph}$ make a sufficient and a necessary condition, respectively, for the occurrence of centrifugal support at the end of major equatorial axis in the case under consideration.

Owing to Newton,s and MacLaurin's theorem, the condition of centrifugal support, Eq. (71), for focaloidally striated ellipsoids surrounded by homeoidally striated coronae, coincides with its counterpart related to homogeneous ellipsoids with equal mean density, axis ratios, and velocity field. On the other hand, the rotation parameter, $\upsilon_{iso}(a_1')$, in the special case of focaloidally striated ellipsoids, is also expressed by Eq. (71), particularized to classical Jacobi ellipsoids. A comparison with the last part of Eq. (71) shows that centrifugal support in focaloidally striated ellipsoids occurs only for flat configurations, $\epsilon_{31} = 0$. Accordingly, Eq. (72) reduces to:

$$0 \leq [\upsilon_{iso}(a_1')]_{eq} \leq \frac{2}{3} \quad ; \tag{73}$$

owing to Eq. (71) and $(A_1)_{sph} = 2/3$ (e.g., CM03).

With regard to rigid rotation, it is a well known result that the occurrence of centrifugal support, at the end of the major equatorial axis, depends on the steepness of the density profile (e.g., Jeans 1929, Chap. IX, §§ 230-240). More precisely, a steeper density profile implies an earlier centrifugal support and vice versa, unless the bifurcation point from ellipdoidal to pear-shaped configurations is attained, which occurs for nearly homogeneous matter distributions. A similar trend is expected to hold for any velocity profile of the kind considered in the current paper.

The combination of Eq. (72) with its counterpart related to the boundary, yields:

$$\upsilon_{iso}(a_1') = \upsilon_{iso} \frac{M}{M(a_1')} \left(\frac{a_1'}{a_1}\right)^3 \frac{\Omega^2(a_1')}{\Omega^2(a_1)} \quad ; \tag{74}$$

a further restriction to mass distributions obeyng the following law:

$$\frac{M(a_1')}{M} = \left(\frac{a_1'}{a_1}\right)^k \quad ; \qquad 0 \leq k \leq 3 \quad ; \tag{75}$$

where $k = 3, 1, 0$, represent homogeneous, isothermal, and Roche-like mass distributions, make Eq. (74) reduce to:

$$\upsilon_{iso}(a_1') = \upsilon_{iso} \left(\frac{a_1'}{a_1} \right)^{3-k} \frac{\Omega^2(a_1')}{\Omega^2(a_1)} \quad ; \tag{76}$$

where the last factor equals unity for rigid rotation and the ratio, $(a_1/a_1')^2$, for constant velocity along the major equatorial axis. Accordingly, centrifugal support at the end of major equatorial axis is first attained on the boundary in the former alternative, $\upsilon_{iso}(a_1') \leq \upsilon_{iso}(a_1)$.

In the latter alternative, Eq. (76) reduces to:

$$\upsilon_{iso}(a_1') = \upsilon_{iso} \left(\frac{a_1'}{a_1} \right)^{1-k} \quad ; \tag{77}$$

which, for sufficiently steep density profiles, $0 \leq k \leq 1$, shows a similar trend with respect to the former alternative. On the other hand, centrifugal support is first attained everywhere along the major equatorial axis for isothermal mass distributions, $k = 1$, and at the centre for sufficiently mild density profiles, $1 \leq k \leq 3$, which implies $\upsilon_{iso}(a_1') \geq \upsilon_{iso}(a_1)$.

The combination of Eqs. (48) and (71) yields:

$$\{[(\upsilon_N)_{iso}(a_1')]_{eq}\}_w = \frac{3\eta_{rot}\nu_{rot}}{\nu_{sel}}(A_1)_w \quad ; \tag{78}$$

and Eq. (73) reads:

$$0 \leq [(\upsilon_N)_{iso}(a_1')]_{eq} \leq \frac{2\eta_{rot}\nu_{rot}}{\nu_{sel}} \quad ; \tag{79}$$

in terms of the normalized rotation parameter, υ_N.

3.6 Bifurcation points

Owing to Theorem 4, a bifurcation point from axisymmetric to triaxial configurations is related to an axis ratio, ϵ_{31}, which is independent of the amount of systematic rotation and residual motion excess, according to Eq. (56). To gain more insight, let us equalize the alternative expressions of Eq. (49). The result is:

$$A_1 - \frac{\zeta_{11}}{\zeta_{33}}\epsilon_{31}^2 A_3 = A_2 - \frac{\zeta_{22}}{\zeta_{33}}\epsilon_{32}^2 A_3 \quad ; \tag{80}$$

and the combination of Eqs. (63) and (80) yields:

$$\frac{A_2 - A_1}{1 - \epsilon_{21}^2} = \frac{\epsilon_{31}^2}{\epsilon_{21}^2} A_3 \quad ; \tag{81}$$

and the bifurcation points occur at a configuration, where the axis ratio, ϵ_{31}, is the solution of the transcendental equation (Caimmi 1996a):

$$\lim_{\epsilon_{21} \to 1} \epsilon_{21}^2 \frac{A_2 - A_1}{1 - \epsilon_{21}^2} = \epsilon_{31}^2 A_3 \quad ; \tag{82}$$

where Eqs. (81) and (82) coincide with their counterparts related to isotropic residual velocity distributions (Caimmi 1996a,b). The above results may be reduced to a single statement.

Theorem 9. *Given a sequence of homeoidally striated Jacobi ellipsoids, the bifurcation point occurs at the same configuration, as in the sequence of classical Jacobi ellipsoids.*

The contradiction with earlier results (Wiegandt 1982a,b; CM05) is explained in the following way. Let us suppose that the generalized anisotropy parameters, $\zeta_{11}, \zeta_{22}, \zeta_{33}$, can be arbitrarily fixed regardless from Eqs. (63), and assume $\zeta_{11} = \zeta_{22}$ *also* for triaxial configurations. Accordingly, Eq. (80) reads:

$$\frac{A_2 - A_1}{1 - \epsilon_{21}^2} = \frac{\zeta_{11}}{\zeta_{33}} \frac{\epsilon_{31}^2}{\epsilon_{21}^2} A_3 \quad ; \tag{83}$$

and the bifurcation points occur at a configuration where the axis ratio, ϵ_{31}, is the solution of the transcendental equation:

$$\lim_{\epsilon_{21} \to 1} \epsilon_{21}^2 \frac{A_2 - A_1}{1 - \epsilon_{21}^2} = \frac{\zeta_{11}}{\zeta_{33}} \epsilon_{31}^2 A_3 \quad ; \tag{84}$$

which coincides with Wiegandt (1982b) criterion for bifurcation, with regard to homeoidally striated Jacobi ellipsoids in rigid rotation. For a formal demonstration, see Appendix B. Then Wiegandt's criterion for bifurcation, expressed by Eq. (84), is in contradiction with Eqs. (63), contrary to the current one, expressed by Eq. (82).

3.7 Interpretation of results from numerical simulations on stability

Given a homeoidally striated Jacobi ellipsoid, the occurrence of anisotropic residual velocity distribution may be related to residual motion excess, via Eqs. (54) and (55). In fact, the changes:

$$(E_{res})_{qq} \to (E_{res})_{qq} - (\Delta E_{res})_{qq} \quad ; \tag{85a}$$

$$(E_{rot})_{qq} \to (E_{rot})_{qq} + (\Delta E_{res})_{qq} \quad ; \tag{85b}$$

$$(\Delta E_{res})_{qq} = (\zeta_{33} - \zeta_{qq}) E_{res} \quad ; \qquad q = 1, 2 \quad ; \tag{85c}$$

do convert (positive or negative) peculiar motion excess into systematic (real or imaginary) rms rotation, and the diagonal components of the residual-energy tensor read $(E_{res})_{pp} \to (E_{res})_{pp} - (\Delta E_{res})_{pp} = (E_{res})_{33}$.

The velocity field related to rms rotation has to coincide with the pre-existing one, apart from a renormalization, defined by Eq. (59), and the mean rotational velocity, $\Omega_{ani}(x_1, x_2, x_3)(x_1^2 + x_2^2)^{1/2}$, has necessarily to be null within any infinitesimal mass element.

In this view, recent results from numerical simulations on the stability of rotating stellar systems (Meza 2002), find a natural interpretation. Each computer run therein proceeds along the following steps.

(i) Take a spherical system with isotropic peculiar velocity distribution and null systematic rotation velocity field.

(ii) Fix a rotation axis, let it be x_3.

(iii) Reverse a selected sense of rotation of a given fraction of the particles, by changing the tangential (parallel to equatorial plane) velocity component, v_ϕ, into its opposite, $-v_\phi$.

(iv) Make the system evolve from the above defined initial configuration.

It is worth noticing (Meza 2002) that the distribution function is independent of the sign of v_ϕ, and the whole set of possible initial configurations under discussion, are characterized by the same total kinetic and potential energy.

The simulations show that spherical systems of the kind considered are dynamically stable, irrispective of their degree of rotation. Even if very rapidly rotating, boundaries fail to become oblate-like.

In the light of the current theory, reversing an assigned sense of rotation of a given fraction of the particles, implies a conversion of a fraction of residual energy into rotational energy, as:

$$\Delta E_{res} = -\Delta E_{rot} = -nm < v_\phi^2 > \quad ; \tag{86}$$

$$< v_\phi^2 >= \frac{1}{n} \sum_{i=1}^{n} \left[v_\phi^{(i)} \right]^2 \quad ; \qquad 0 \leq n \leq \frac{N}{2} \quad ; \tag{87}$$

$$\sum_{i=1}^{N-2n} v_\phi^{(i)} = 0 \quad ; \qquad n \ll \frac{N}{2} \quad ; \tag{88}$$

where n is the number of particles with reversed tangential (parallel to the equatorial plane) velocity component, N is the total number of particles, and m is the mass, assumed to be equal for each particle, as done in numerical simulations (Meza 2002). The validity of Eq. (88) does not necessarily rule out streaming motions other than systematic rotation. On the contrary, streaming motions are allowed provided the existence of a given flow implies a counter-flow, such that Eq. (88) is satisfied.

Before reverting the sense of rotation, the following relations hold in consequence of isotropic residual velocity distribution:

$$< v_1^2 >=< v_2^2 >=< v_3^2 > \quad ; \tag{89a}$$

$$< v_\phi^2 > + < v_w^2 >=< v_1^2 > + < v_2^2 > \quad ; \tag{89b}$$

where v_p, $p = 1, 2, 3$, and v_w, $w = (x_1^2 + x_2^2)^{1/2}$, are velocity components parallel to coordinate axes and equatorial plane, respectively. After reversion of the sense of rotation, the following changes are performed:

$$E_{res} \rightarrow E_{res} - nm < v_\phi^2 > \quad ; \tag{90}$$

$$(E_{res})_\phi \rightarrow (E_{res})_\phi - nm < v_\phi^2 > \quad ; \tag{91}$$

$$(E_{res})_{qq} \rightarrow (E_{res})_{qq} - \frac{1}{2} nm < v_\phi^2 > \quad ; \qquad q = 1, 2 \quad ; \tag{92}$$

$$E_{rot} \rightarrow 0 + nm < v_\phi^2 > \quad ; \tag{93}$$

$$(E_{rot})_{qq} \rightarrow 0 + \frac{1}{2} nm < v_\phi^2 > \quad ; \qquad q = 1, 2 \quad ; \tag{94}$$

while the contributions from residual motions along the equatorial plane, $(E_{res})_w$, and the rotation axis, $(E_{res})_{33}$, remain unchanged.

The system being relaxed, $\zeta = 1$, in the case under discussion, the generalized and effective anisotropy parameters, ζ_{pp} and $\tilde{\zeta}_{pp}$, coincide with their usual counterparts, and Eqs. (23) and (26) take the explicit form:

$$\zeta_{qq} = \frac{(E_{res})_{qq} - (n/2)m < v_\phi^2 >}{(E_{res}) - nm < v_\phi^2 >} \quad ; \qquad q = 1, 2 \quad ; \tag{95a}$$

$$\zeta_{33} = \frac{(E_{res})_{33}}{(E_{res}) - nm < v_\phi^2 >} \quad ; \tag{95b}$$

where the special case, $n = 0$, turns back to isotropic residual velocity distributions, $\zeta_{11} = \zeta_{22} = \zeta_{33} = 1/3$.

In the extreme case where the sense of rotation is completely reversed, $n = N/2$, the changes expressed by Eqs. (90)-(94) reduce to:

$$E_{res} \to E_{res} - \frac{N}{2} m < v_\phi^2 >= \frac{2}{3} E_{res} \quad ; \tag{96}$$

$$(E_{res})_\phi \to (E_{res})_\phi - \frac{N}{2} m < v_\phi^2 >= 0 \quad ; \tag{97}$$

$$(E_{res})_{qq} \to (E_{res})_{qq} - \frac{N}{4} m < v_\phi^2 >= \frac{1}{6} E_{res} \quad ; \qquad q = 1, 2 \quad ; \tag{98}$$

$$E_{rot} \to 0 + \frac{N}{2} m < v_\phi^2 >= \frac{1}{3} E_{res} \quad ; \tag{99}$$

$$(E_{rot})_{qq} \to 0 + \frac{N}{4} m < v_\phi^2 >= \frac{1}{6} E_{res} \quad ; \qquad q = 1, 2 \quad ; \tag{100}$$

and the anisotropy parameters, expressed by Eqs. (95), reduce to:

$$\zeta_{qq} = \frac{(1/6)E_{res}}{(2/3)E_{res}} = \frac{1}{4} \quad ; \qquad q = 1, 2 \quad ; \tag{101a}$$

$$\zeta_{33} = \frac{(1/3)E_{res}}{(2/3)E_{res}} = \frac{1}{2} \quad ; \tag{101b}$$

which describes the maximum amount of residual motion excess, related to complete reversion of the sense of the rotation.

Turning back to the general case, a comparison between the expression of rotational energy, Eq. (15), with the special one related to the case under discussion, Eq. (93), reads:

$$\eta_{rot}\nu_{rot} M (1 + \epsilon_{21}^2) < v_\phi^2 >_{a_1} = nm < v_\phi^2 > \quad ; \tag{102}$$

where $< v_\phi^2 >_{a_1}$ is the rms systematic rotation velocity at the end of the major equatorial
axis [7], $w = (x_1^2 + x_2^2)^{1/2} = a_1$. The related rms angular velocity is:

$$\Omega^2 = \Omega^2(a_1) = \frac{< v_\phi^2 >_{a_1}}{a_1^2} \quad ; \tag{103}$$

and the combination of Eqs. (5), (6), (22), (34), (35), (48), (88), (102), and (103) yields after some algebra:

$$\upsilon_N = \frac{2nm < v_\phi^2 > a_1 \epsilon_{21} \epsilon_{31}}{\nu_{sel} GM^2 (1 + \epsilon_{21}^2)} = -\frac{B_{sel} \epsilon_{21} \epsilon_{31}}{1 + \epsilon_{21}^2} \frac{\Delta E_{res}}{E} \quad ; \tag{104}$$

where $E = E_{sel}/2$ is the total energy, according to the virial theorem. On the other hand, the combination of Eqs. (55), (88), and (95) yields:

$$(\upsilon_N)_{ani} = -\frac{3nm < v_\phi^2 >}{E_{res}} \frac{\epsilon_{31}^2 A_3}{1 + \epsilon_{21}^2} = -3 \frac{\epsilon_{31}^2 A_3}{1 + \epsilon_{21}^2} \frac{\Delta E_{res}}{E} \quad ; \tag{105}$$

where $E = -E_{res}$ is the total energy, according to the virial theorem.

The validity of the above results is related to the assumption of relaxed configurations, which implies a virial index, $\zeta = 1$, according to Eqs. (22), (23), and (24). In addition, the assumption of sphericity necessarily restricts the validity of Eqs. (104) and (105) to spherical systems, where $\epsilon_{21} = \epsilon_{31} = 1$, $A_1 = A_2 = A_3 = 2/3$, $B_{sel} = 2$. Accordingly, the expression of the rotation parameters, υ_N and $(\upsilon_N)_{ani}$, reduces to:

$$\upsilon_N = \frac{\Delta E_{res}}{E} \quad ; \qquad (\upsilon_N)_{ani} = -\frac{\Delta E_{res}}{E} \quad ; \tag{106}$$

which implies an adjoint spherical configuration with rotation parameter, $(\upsilon_N)_{iso} = \upsilon_N + (\upsilon_N)_{ani} = 0$, as expected. This is why an additional real rotation, due to the change $E_{rot} \rightarrow E_{rot} - \Delta E_{res}$, is exactly balanced by an additional imaginary rotation, due to the change $E_{res} \rightarrow E_{res} + \Delta E_{res}$, according to Eqs. (106). Then the initial shape remains unchanged. In addition, owing to Theorem 4, the condition of stability is also expected to be

[7] With the additional restriction, that streaming motions within the volume element at the end of major equatorial axis are allowed provided the existence of a given flow therein implies a counter-flow, such that Eq. (88) is satisfied in the region of interest.

left unaltered. In other words, the rotating sphere ($\zeta_{11} = \zeta_{22} < \zeta_{33}$) is expected to be as stable as the nonrotating sphere ($\zeta_{11} = \zeta_{22} = \zeta_{33}$), regardless from the assumed density profile, according to the results from numerical simulations (Meza 2002).

4 Application: physical interpretation of the early Hubble sequence

The results of the current paper allow an extension and a generalization to anisotropic peculiar velocity distributions, of the classical physical interpretation of the Hubble (1926) sequence (e.g., Jeans 1929, Chap. XIII, §§ 298-303). In the following, quotations are from therein. Owing to Theorem 4, it will suffice to restrict to solid-body rotating configurations with isotropic peculiar velocity distributions, but with imaginary rotation also taken into consideration.

4.1 Classification of galaxies

It is worth recalling that, before establishing their similarity to the Milky Way, galaxies were referred to as "great nebulae" or "nebulae".

> Hubble finds that it is not possible to place all observed nebulae in one continuous sequence; their proper representation demands a Y-shaped diagram. (...)
>
> The lower half of the Y is formed by nebulae of approximately elliptical or circular shape. These are subdivided into eight classes, designated $E0$, $E1$, ..., $E7$, the numerical index being the integer nearest to $10[(a-b)/a]$, where a and b are the greatest and the least diameter of the nebulae as projected on the sky. Thus $E0$ consists of nearly circular nebuale ($b > 0.95a$), while $E7$ consists of nebulae for which b is about $0.3a$, this being the greatest inequality of axes observed in the "elliptical" nebulae. (...)
>
> The upper half of the Y-shaped diagram consists of two distinct branches, one of which is found to contain a far larger number of nebulae than in the other. The principal branch contains

the normal "spiral" nebulae, which are characterized by a circular nucleus from which emerge two (or occasionally more) arms of approximately spiral shape. (...) These nebulae are subdivided into three classes, designated Sa, Sb, Sc, class Sa fitting almost continuously on to class $E7$.

The minor branch contains a special class of spirals characterized by the circumstance that the spiral arms appear to emerge from the two ends of a straight bar-shaped or spindle-shaped mass. (...)

About 97 per cent of known extra-galactic nebulae are found to fit into this Y-shaped classification. The remaining 3 per cent, are of irregular shape, and refuse to fit into the classification at all. (...) The irregular nebulae are distinguished by a complete absence of symmetry of figure and also by the absence of any central nucleus. (...)

Apart from the irregular nebulae, Hubble states that, out of more than a thousand nebulae examined, less than a dozen refused to fit into the Y-shaped diagram at all, while in less than 10 per cent of the cases was there any considerable doubt as to a proper position of a nebula in the diagram. Clearly, the Y-shaped diagram provides a highly satisfactory working classification.

Thought some improvements have been made to the classification of galaxies (e.g., van den Bergh 1960a,b; Roberts & Haynes 1994), still we shall maintain Hubble (1926) diagram as a valid point of reference, owing to its intrinsic simplicity.

4.2 Physical interpretation

Obviously the proper physical interpretation of the classification just described is of the utmost importance to cosmogony.

A first and most important clue is provided by the fact that numbers of the great nebulae are known to be in rotation. (...)

The symmetry of figure shewn by nebulae of the E and Sa types is precisely such as rotation might be expected to produce, and this suggests an inquiry as to how far the observed figures of

> the regular nebulae can be explained as the figures assumed by masses rotating under their own gravitation. (...)
>
> Remembering that rotation has actually been observed in a number of nebulae, there seem to be strong reasons for conjecturing that the observed configuration of the nebulae may be explained in general terms as the configurations of rotating masses.

More specifically, two classes of models are considered, where density profiles range between the limiting cases (i) homogeneous configurations i.e. classical MacLaurin spheroids and Jacobi ellipsoids, and (ii) mass points surrounded by massless atmospheres i.e. Roche systems. Rigidly rotating mass distributions of the kind considered may attain any shape between the extreme boundaries (a) spherical i.e. nonrotating, and (b) centrifugal support at the end of major equatorial axis. With respect to the latter configuration, further rotation implies equatorial shedding (sequence SN) or top major equatorial axis streaming (sequenceSB) of matter, for axisymmetric and triaxial configurations, respectively. For a fixed density profile, the sequence of rigidly rotating configurations starts from the spherical shape and ends at the shape where centrifugal support is first attained.

The above interpretation suffers from two main points. First, the most flattened elliptical configuration should occur when centrifugal support takes place at the bifurcation point, from axisymmetric to triaxial shapes. On the other hand, the above mentioned limiting configuration is less flattened than $E7$. Second, triaxial bodies of the kind considered cannot be figures of equilibrium if a great central condensation of mass is present. On the other hand, it is the case for barred spirals.

Owing to Theorem 4, homeoidally striated Jacobi ellipsoids with arbitrary peculiar velocity field, and systematic motions reduced to rotation around a fixed axis, may be related to classical Jacobi ellipsoids, provided imaginary rotation is taken into consideration. Then the occurrence of anisotropic peculiar velocity distributions does not affect the physical interpretation under discussion, and the questions to be clarified are the above mentioned two.

4.3 The E sequence within Ellipsoidland

In dealing with a physical interpretation of the early Hubble sequence, it is convenient to define axis ratios of intrinsic configurations in a different way.

Given a homeoidally striated Jacobi ellipsoid, let a, b, c, be the semiaxes, where $a \geq b \geq c$ without loss of generality. Accordingly, $\epsilon_{ca} \leq \epsilon_{ba} \leq 1$; in addition, the minor and the major axis coincide with the rotation axis for oblate-like and prolate-like configurations, respectively.

The whole range of possible configurations in the $(\mathsf{O}\epsilon_{ba}\epsilon_{ca})$ plane defines Ellipsoidland (the term is from Hunter & de Zeeuw 1997). Ellipsoidland is a triangle where two sides are of unit length and an angle is right, as shown in Fig. 3. Oblate configurations lie on the vertical side, $\epsilon_{ba} = 1$, the spherical configuration is on the top, $\epsilon_{ca} = 1$, and the flat circular configuration is on the bottom, $\epsilon_{ca} = 0$. Prolate configurations lie on the inclined side, $\epsilon_{ca} = \epsilon_{ba}$, the spherical configuration is on the top, $\epsilon_{ca} = \epsilon_{ba} = 1$, and the prolate oblong configuration is on the bottom, $\epsilon_{ca} = \epsilon_{ba} = 0$. Flat configurations lie on the horizontal side, $\epsilon_{ca} = 0$, the flat circular configuration is on the right, $\epsilon_{ba} = 1$, and the flat oblong configuration is on the left, $\epsilon_{ba} = 0$. It is worth noticing that flat-oblong and prolate-oblong configurations are not coincident (e.g., Caimmi 1993; CM05). Non flat, non axisymmetric configurations, lie within Ellipsoidland.

The axis ratio correlation, ϵ_{ca} vs. ϵ_{ba}, related to adjoint configurations to homeoidally striated Jacobi ellipsoids, is represented within Ellipsoidland in Fig. 3. The caption of symbols is the same as in Fig. 1. With regard to real rotation, the correlation is the known one involving classical MacLaurin spheroids and Jacobi ellipsoids. With regard to imaginary rotation, the correlation reads $\epsilon_{ca} = \epsilon_{ba}$, owing to lack of bifurcation points. Then configurations in real and imaginary rotation branch off from the nonrotating spherical configuration. The former sequence proceeds down along the oblate side of Ellipsoidland, until the bifurcation point is attained and the curve enters Ellipsoidland, finishing when the next bifurcation point is also attained. The latter sequence proceeds down along the prolate side of Ellipsoidland, until the prolate-oblong configuration is attained, never entering Ellipsoidland. On the other hand, a sequence may stop earlier, when centrifugal support at the ends of major equatorial axis is attained, which depends on the density profile. In fact, it makes the sole difference between homeoidally striated Jacobi ellipsoids and their adjoint counterparts (for further details, see CM05).

With regard to Ellipsoidland, the observed lack of elliptical galaxies more flattened than $E7$ translates into the inequality, $\epsilon_{ca} \geq 0.25$, the treshold being represented by the lower dashed horizontal line in Fig. 3. The locus of

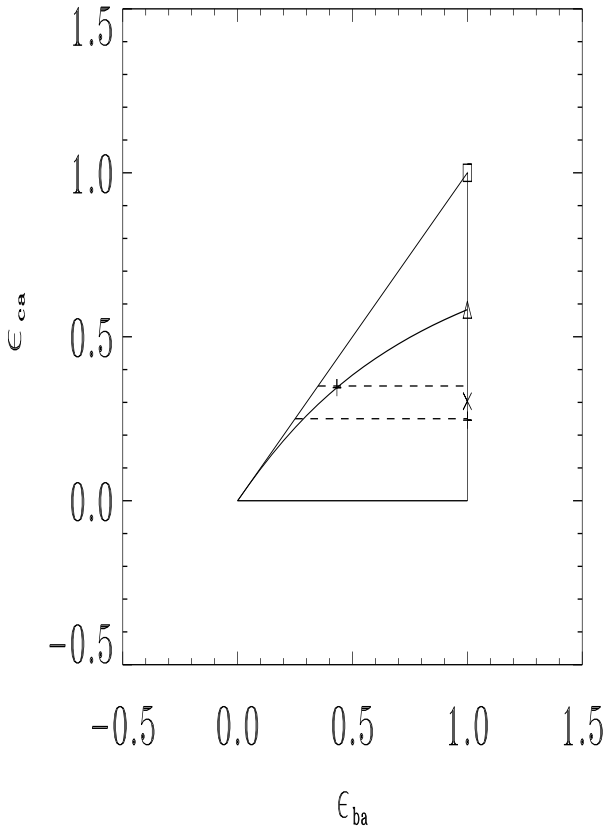

Figure 3: Axis ratio correlation within Ellipsoidland, with regard to adjoint configurations to homeoidally striated Jacobi ellipsoids. The semiaxes are a, b, c, where $a \geq b \geq c$ or $\epsilon_{ca} \leq \epsilon_{ba} \leq 1$, without loss of generality. The locus of flat configurations is $\epsilon_{ca} = 0$, $0 \leq \epsilon_{ba} \leq 1$. The locus of oblate configurations is $\epsilon_{ba} = 1$, $0 \leq \epsilon_{ca} \leq 1$. The spherical configuration is defined as $\epsilon_{ca} = \epsilon_{ba} = 1$. The oblong configuration is defined as $\epsilon_{ca} = \epsilon_{ba} = 0$. The locus of prolate configurations is $\epsilon_{ca} = \epsilon_{ba}$, $0 \leq \epsilon_{ba} \leq 1$. Different configurations occur in the flat oblong limit, $\epsilon_{ca} = 0$, $\epsilon_{ba} \to 0$, and in the prolate oblong limit, $\epsilon_{ca} \to 0$, $\epsilon_{ba} \to 0$, $\epsilon_{ca} = \epsilon_{ba}$. A band, bounded by two horizontal dashed lines, defines class $E7$ in Hubble (1926) classification i.e. $0.25 < \epsilon_{ca} \leq 0.35$ for edge-on ellipsoids where the line of sight coincides with the direction of the minor equatorial axis. Other symbols as in Fig. 1.

edge-on configurations, viewed along a direction coinciding with equatorial minor axis, where $0.25 \leq \epsilon_{ca} \leq 0.35$, and then belonging to class $E7$, is represented in Fig. 3 as a band bounded by two dashed lines, $\epsilon_{ca} = 0.25$ and $\epsilon_{ca} = 0.35$, respectively. A change in direction of the line of sight could project an intrinsic ellipsoid within the above mentioned band, on a class Ei, $i < 7$.

An inspection of Fig. 3 shows that the bifurcation points from triaxial and axisymmetric configurations, towards pear-shaped configurations, are consistent, or marginally consistent, with the $E7$ band on Ellipsoidland. The above considerations provide a physical interpretation to the observed absence of elliptical galaxies (and spiral bulges) more flattened than $E7$, with regard to the oblate-like branch of the sequence. On the other hand, the above interpretation cannot apply to the prolate branch of the sequence, as no bifurcation point has been found therein, and some kind of instability must be considered.

The absence of elliptical galaxies more flattened or elongated than $E7$ might be due to bending instabilities, as suggested long time ago from analytical considerations involving homogeneous (oblate and prolate) spheroids (Polyachenko & Shukhman 1979; Fridman & Polyachenko 1984, Vol. 1, Chap. 4, Sect. 3.3, see also pp. 313-322; Vol. 2, p. 159) and numerical simulations involving inhomogeneous (oblate and prolate) spheroids (Merritt & Hernquist 1991; Merritt & Sellwood 1994). The amount of figure rotation seems to be unimportant to this respect (Raha et al. 1991; Merritt & Sellwood 1994).

This conclusion is supported by recent results from N-body numerical simulations, where spherically symmetric, unstable, radially anisotropic, one-component γ models were taken as starting configurations (Nipoti et al. 2002). The related end-products, in accordance with previous results (e.g., Merrit & Aguilar 1985; Stiavelli & Sparke 1991), were found to be in general prolate systems less flattened than $E7$ (Nipoti et al. 2002, Fig. 1 therein).

The theoretical explanation of the result, in terms of a dynamical bending instability (Merritt & Sellwood 1994), is generally recognized to explain also the maximum elongation of simulated nonbaryonic dark matter haloes (e.g., Bett et al. 2007).

4.4 Tidal effects from hosting dark matter haloes

Current ΛCDM cosmologies, which provide a satisfactory fit to data from primordial nucleosynthesis and cosmic background radiation, predict galaxies are embedded within dark matter haloes. Then it is a natural question to what extent the presence of hosting dark matter haloes may affect the above interpretation of the early Hubble sequence. To this aim, an idealized situation shall be analysed.

Let us represent elliptical galaxies and their hosting dark haloes as concentric and coaxial classical Jacobi ellipsoids, one completely lying within the other. Accordingly, the two bodies must necessarily rotate at the same extent, and/or one of them (the outer in the case under discussion) has to be axisymmetric. It can be seen that the effect of the outer ellipsoid on the inner one is to shift bifurcation points towards more flattened configurations with respect to a massless embedding subsystem (Durisen 1978; Pacheco et al. 1986; Caimmi 1996a).

More specifically, the axis ratio of the configuration at the bifurcation point is the solution of the transcendental equation (Caimmi 1996a):

$$\frac{[(\epsilon_i)_{31}]^2 (A_i)_3}{(A_i)_1} = \left[\frac{5 - 4[(\epsilon_i)_{31}]^2}{3 - 2[(\epsilon_i)_{31}]^2} + \frac{m}{y_1 y_2 y_3} \frac{4 - 4[(\epsilon_i)_{31}]^2}{3 - 2[(\epsilon_i)_{31}]^2} \frac{(A_j)_3}{(A_i)_3} \right]^{-1} \quad ; \tag{107a}$$

$$m = \frac{M_j}{M_i} \quad ; \qquad y_k = \frac{(a_j)_k}{(a_i)_k} \quad ; \qquad \frac{m}{y_1 y_2 y_3} = \frac{\rho_j}{\rho_i} \quad ; \tag{107b}$$

where the indices, i, j, denote inner and outer ellipsoid, respectively.

The effect of the embedding subsystem on the shape of the embedded configuration at the bifurcation point, is governed by the parameter:

$$\kappa = \frac{m}{y_1 y_2 y_3} \frac{(A_j)_3}{(A_i)_3} \quad ; \qquad 0 \leq \kappa < +\infty \quad ; \tag{108}$$

in the special case of massless outer ellipsoid, $\kappa = 0$, Eq. (107a) reduces to (65).

Further analysis shows that the embedded configuration, at the bifurcation point, is as flattened as $E7$ when the parameter, κ, is close to unity. Accordingly, the following relation holds:

$$\frac{m}{y_1 y_2 y_3} \frac{(A_j)_3}{(A_i)_3} = 1 \quad ; \qquad 0.25 < (\epsilon_i)_{31} \leq 0.35 \quad ; \tag{109}$$

where the shape factor ratio, $(A_j)_3/(A_i)_3$, exceeds unity if the outer ellipsoid is more flattened than the inner one, and vice versa.

The generalization of Eq. (109) to homeoidally striated Jacobi ellipsoids demands to restart from a generalized formulation of the virial theorem, where the tidal potential is also included (Brosche et al. 1983; Caimmi et al. 1984; Caimmi & Secco 1992). The repetition of the same procedure used in the current paper, yields:

$$\frac{m}{y_1 y_2 y_3} \frac{(\nu_{ij})_{tid}}{(\nu_i)_{sel}} \frac{(A_j)_3}{(A_i)_3} = 1 \quad ; \qquad 0.25 < (\epsilon_i)_{31} \leq 0.35 \quad ; \tag{110}$$

where $(\nu_{ij})_{tid}$ is an additional factor in the expression of the potential tidal energy, related to the tidal action of the embedding subsystem on the embedded one (Caimmi 2003; CM05).

It may safely be expected that the external boundary is less flattened than the internal one and more flattened than a sphere. Accordingly, the shape factor ratio appearing in Eqs. (109), (110), ranges as $1/2 < (A_j)_3/(A_i)_3 < 1$ for oblate configurations, and $1 < (A_j)_3/(A_i)_3 < 10/3$ for prolate configurations. Then, to a first extent, $(A_j)_3/(A_i)_3 \approx 1$, i.e. the boundaries are similar and similarly placed ellipsoids. With this restriction, the factor, $(\nu_{ij})_{tid}$, is a profile factor, which may be expressed by a simple formula (Caimmi 2003):

$$(\nu_{ij})_{tid} = -\frac{9}{8} \frac{m \Xi_i}{(\nu_i)_{mas} (\nu_j)_{mas}} w^{(ext)} \frac{\Xi_i}{y_0} \quad ; \tag{111}$$

where y_0 is the scaling radius ratio of outer to inner subsystem, and $w^{(ext)}(\eta)$ is an additional profile factor.

Typical elliptical galaxies and their hosting dark haloes may safely be represented as homeoidally striated Jacobi ellipsoids, where the star and dark subsystem are described by generalized power-law density profiles of the kind:

$$f(\xi_u) = \frac{2^\chi}{\xi_u^\gamma (1 + \xi_u^\alpha)} \quad ; \qquad \chi = \frac{\beta - \gamma}{\alpha} \quad ; \qquad u = i, j \quad ; \tag{112a}$$

$$\xi_u = \frac{r_u}{(r_0)_u} \quad ; \qquad \Xi_u = \frac{R_u}{(r_0)_u} \quad ; \tag{112b}$$

$$\xi_i = y_0 \xi_j \quad ; \qquad y \Xi_i = y_0 \Xi_j \quad ; \tag{112c}$$

$$y_0 = \frac{(r_0)_j}{(r_0)_i} \quad ; \qquad y = \frac{R_j}{R_i} \quad ; \tag{112d}$$

according to Eqs. (1), and the choices $(\alpha, \beta, \gamma) = (1, 4, 1)$ (Hernquist 1990) and $(\alpha, \beta, \gamma) = (1, 3, 1)$ (Navarro et al. 1995, 1996, 1997) are adopted to describe the star and the dark subsystem, respectively. The values of input and output parameters of the model are listed in Tab. 1, with regard to a ΛCDM cosmology where $\Omega_M = 0.3$, $\Omega_\Lambda = 0.7$, $\Omega_b = 0.0125h^{-2}$, $h = 2^{-1/2}$. For further details and references, see CM05.

The presence of a massive halo has little influence on the location of the bifurcation point from axisymmetric to triaxial configurations, which is found to occur at an axis ratio, $(\epsilon_{31})_{bif} = 0.580088$. A similar result is expected to occur for the bifurcation point from both axisymmetric and triaxial to pear-shaped configurations. Then the above mentioned points continue to be consistent, or marginally inconsistent, with the $E7$ band on Ellipsoidland, even in presence of (typical) massive dark haloes, concerning the oblate-like branch of the sequence. On the contrary, it is suggested the existence of some kind of instability, which does not allow prolate configurations in rigid imaginary rotation, more elongated than $E7$, even in presence of (typical) massive dark haloes, according to recent results from N-body simulations (Nipoti el al., 2002).

4.5 Cosmological effects after decoupling

About thirthy years ago, Thuan & Gott (1975) idealized elliptical galaxies as MacLaurin spheroids, resulting from virialization after cosmological expansion and subsequent collapse and relaxation of their parent density perturbation. A generalization of the method to triaxial configurations and anisotropic peculiar velocity distributions, has been performed in CM05, and an interested reader is addressed therein for further details. Owing to Theorem 4, the case of isotropic peculiar velocity distribution, involving both real and imaginary rotation, can be considered without loss of generality.

Our attention shall be limited to dark matter haloes hosting giant galaxies, as massive as about $10^{12} m_\odot$. Accordingly, it is assumed $\overline{\delta}_{rec} = 0.015$ as a typical overdensity index of the initial configuration, taken to be at recombination epoch, and a relaxed final configuration i.e. $\zeta = 1$.

With regard to the initial configuration, the following approximations hold to a good extent: (i) spherical shape; (ii) homogeneous mass distribution; (iii) negligible (real and/or imaginary) rotation energy; (iv) negligible peculiar energy. The changes in mass, angular momentum, and total energy,

input	value	output	value
Ξ_i	40/3	$(\nu_i)_{mas}$	10.38399
Ξ_j	10	$(\nu_j)_{mas}$	17.86565
$(r_0)_i$/kpc	3.21	$(\nu_i)_{sel}$	1.44444
$(r_0)_j$/kpc	36.20	$(\nu_j)_{sel}$	0.6268271
R_i/kpc	42.77	$(\nu_{ij})_{tid}$	0.3518317
R_j/kpc	362.04	$(\nu_{ji})_{tid}$	0.2217760
$M_i/10^{10}m_\odot$	8.33	$(\nu_i)_{rot}$	1/3
$M_j/10^{10}m_\odot$	91.67	$(\nu_j)_{rot}$	1/3
y_0	11.29	$(\eta_i)_{rot}$	1/2
y	8.47	$(\eta_j)_{rot}$	1/2
m	11	$w^{(est)}$	-0.3955800
		$w^{(int)}$	-3.564028
		$(\nu_{ij})_{int}$	1.760852
		$(\nu_{ji})_{int}$	1.760852
		$\left(\frac{2\eta_{rot}\nu_{rot}}{\nu_{sel}}\right)_i$	0.230769
		$\left(\frac{2\eta_{rot}\nu_{rot}}{\nu_{sel}}\right)_j$	0.531779
		$\frac{m}{y^3}\frac{(\nu_{ij})_{tid}}{(\nu_i)_{sel}}$	0.00441624
		$(\epsilon_{31})_{bif}$	0.580088

Table 1: Values of input and output parameters in modelling elliptical galaxies and their hosting dark haloes as similar and similarly placed, homeoidally striated Jacobi ellipsoids, characterized by Hernquist (1990) and Navarro et al. (1995, 1996, 1997) density profiles, respectively. The parameters of the related ΛCDM cosmology have been chosen as $\Omega_M = 0.3$, $\Omega_\Lambda = 0.7$, $\Omega_b = 0.0125h^{-2}$, $h = 2^{-1/2}$. For further details on the output parameters see e.g., CM03.

respectively, during the transition from the initial to final configuration, are expressed by the parameters:

$$\beta_M = \frac{M}{M'} \quad ; \qquad \beta_J = \frac{J}{J'} \quad ; \qquad \beta_E = \frac{E}{E'} \quad ; \tag{113}$$

where the initial configuration is marked by the prime. For further details, see CM05.

Though negligible with respect to the potential and expansion energy, the rotation energy of the initial configuration affects the shape of the final configuration, as:

$$\mathcal{E}'_{rot} = b \mp (b^2 - c)^{1/2} \quad ; \tag{114a}$$

$$b = \frac{1}{2}(1 - \mathcal{E}'_{osc} - \mathcal{E}'_{pec}) \quad ; \tag{114b}$$

$$c = \beta_{\mathcal{E}} \left(\frac{\mathcal{S}}{\mathcal{S}'}\right)^2 \frac{\mathcal{R}'}{\mathcal{R}} \mathcal{E}_{rot} \left[\frac{2\zeta - 1}{2\zeta} - \frac{\zeta - 1}{\zeta}\mathcal{E}_{rot}\right] \quad ; \tag{114c}$$

$$\beta_{\mathcal{E}} = \frac{\beta_M^5}{\beta_J^2 \beta_E} \quad ; \tag{114d}$$

$$\mathcal{E}_{osc} = -\frac{E_{osc}}{E_{sel}} \quad ; \qquad \mathcal{E}_{pec} = -\frac{E_{pec}}{E_{sel}} \quad ; \tag{114e}$$

where different changes in mass, angular momentum, and tidal energy, are related to a same final shape for an assigned initial configuration, provided $\beta_{\mathcal{E}}$ does not vary. The choice, $\beta_{\mathcal{E}} = 1/3600$, in particular $(\beta_M, \beta_J, \beta_E) = (1, 60, 1)$, holds for dark matter haloes hosting giant elliptical galaxies, and it shall be assumed here. For further details, see CM05.

The axis ratios of the final configuration, ϵ_{31} and ϵ_{21}, as a function of the parameter, $\kappa_{\mathcal{E}} = \mathcal{E}'_{rot}/(1 - \mathcal{E}'_{osc} - \mathcal{E}'_{pec})$, are plotted in Fig. 4, with regard to a Navarro et al. (1995,1996,1997) density profile ($\Xi = 9.20678$; see CM05, Tab. 1 therein, for further details) in rigid rotation. Each curve is symmetric with regard to a vertical axis, $\kappa_{\mathcal{E}} = 0.5$, where a local minimum is attained. The plane, $(\mathsf{O}\kappa_{\mathcal{E}}\epsilon)$, may be divided into three regions, namely (a) $0.163190 \leq \kappa_{\mathcal{E}} \leq 0.836810$, where triaxial configurations occur, ranging from $(\epsilon_{21}, \epsilon_{31}) = (1, 0.582724)$ to $(\epsilon_{21}, \epsilon_{31}) = (0.363174, 0.302297)$, the latter related to $\kappa_{\mathcal{E}} = 0.5$; (b) $0 \leq \kappa_{\mathcal{E}} \leq 0.163190$, $0.836810 \leq \kappa_{\mathcal{E}} \leq 1$, where oblate configurations occur, ranging from $(\epsilon_{21}, \epsilon_{31}) = (1, 0.582724)$ to $(\epsilon_{21}, \epsilon_{31}) = (1, 1)$, the latter related to $\kappa_{\mathcal{E}} = 0$ (bound), $\kappa_{\mathcal{E}} = 1$ (unbound), respectively; (c) $-\infty <$

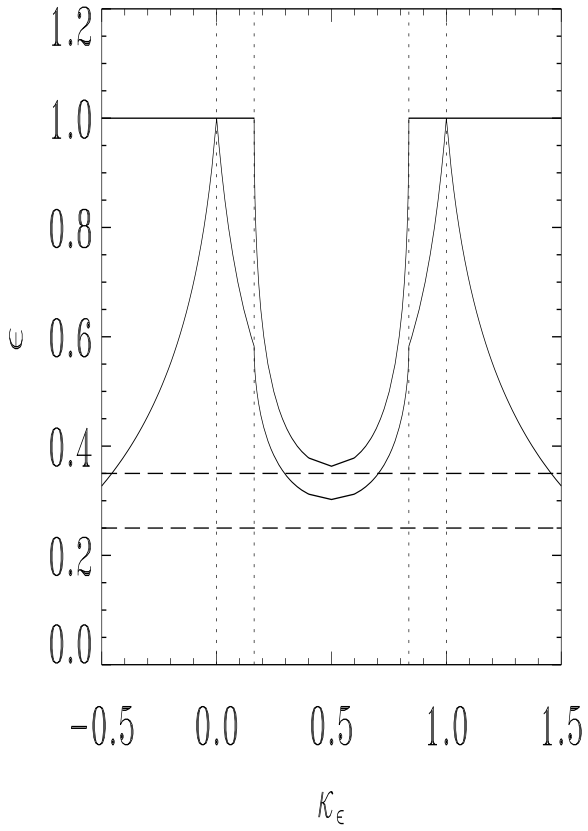

Figure 4: Equatorial (upper curve) and meridional (lower curve) axis ratio of the final configuration, as a function of the parameter, $\kappa_{\mathcal{E}} = \mathcal{E}'_{rot}/(1 - \mathcal{E}'_{osc} - \mathcal{E}'_{pec})$, for sequences of relaxed Navarro et al. (1995, 1996, 1997) density profiles in rigid rotation, related to dark matter haloes hosting giant elliptical galaxies. The curves are symmetric with respect to a vertical axis, $\kappa_{\mathcal{E}} = 0.5$, and a minimum extremum point occurs at $(\kappa_{\mathcal{E}}, \epsilon_{21}, \epsilon_{31}) = (0.5, 0.363174, 0.302297)$, corresponding to the most flattened, oblate-like configuration which is allowed. Values of $\kappa_{\mathcal{E}}$ within or outside the range, $0 \leq \kappa_{\mathcal{E}} \leq 1$, are related to real or imaginary rotation, respectively. Values of $\kappa_{\mathcal{E}}$ below or not below unity, are related to bound (finite extent) and unbound (infinite extent) configurations, respectively. Oblate-like ($\epsilon_{31} \leq \epsilon_{21} \leq 1$) triaxial configurations lie between the inner, vertical dotted lines. Oblate ($\epsilon_{31} \leq \epsilon_{21} = 1$) axisymmetric configurations lie between the inner and the corresponding outer, vertical dotted lines. Prolate ($\epsilon_{21} = 1 \leq \epsilon_{31}$) axisymmetric configurations lie outside the outer, vertical dotted lines. The equatorial axis ratio is $\epsilon = \epsilon_{21}$. The polar axis ratio is $\epsilon = \epsilon_{31}$ for oblate and $\epsilon = \epsilon_{13}$ for prolate configurations. The horizontal dashed lines define class $E7$ in Hubble (1926) classification i.e. $0.25 < \epsilon \leq 0.35$ for edge-on ellipsoids where the line of sight coincides with the direction of the minor equatorial

$\kappa_{\mathcal{E}} \leq 0$, $1 \leq \kappa_{\mathcal{E}} < +\infty$, where prolate configurations occur, ranging from $(\epsilon_{21}, \epsilon_{31}) = (1, 1)$ to $(\epsilon_{21}, \epsilon_{31}) = (1, +\infty)$, the latter related to $\kappa_{\mathcal{E}} \to -\infty$ (bound), $\kappa_{\mathcal{E}} \to +\infty$ (unbound), respectively. It is worth recalling that oblate-like ($\epsilon_{31} \leq \epsilon_{21} \leq 1$) and prolate-like ($\epsilon_{21} \leq 1 \leq \epsilon_{31}$) configurations, are related to real and imaginary rotation, respectively.

An inspection of Fig. 4 shows that, in the case under discussion, cosmological effects due to expansion prevent dark matter haloes in real rotation from being more flattened than $E7$ (dashed horizontal band). The same holds for embedded giant elliptical galaxies, provided the related shapes may safely be thought of as similar and similarly placed. On the other hand, an arbitrary flattening can be attained by dark matter haloes in imaginary rotation, unless some kind of instability occurs, which similarly prevents configurations more elongated than $E7$.

As outlined in Subsect. 4.3, bending instabilities have been suggested long time ago as a viable mechanism to this respect (Polyachenko & Shukhman 1979; Fridman & Polyachenko 1984, Vol. 1, Chap. 4, Sect. 3.3, see also pp. 313-322; Vol. 2, p. 159; Merritt & Hernquist 1991; Merritt & Sellwood 1994).

The above results depend on both density profile and rotation velocity profile of the final configuration, via the coefficient, c, appearing in Eq. (114a). Owing to Eqs. (7) and (17c), Eq. (114c) translates into:

$$c = \beta_{\mathcal{E}'} \frac{\mathcal{R}'}{(\mathcal{S}')^2} \frac{(B_{sel})^2}{B_{ram}} \mathcal{E}_{rot} \left[\frac{2\zeta - 1}{2\zeta} - \frac{\zeta - 1}{\zeta} \mathcal{E}_{rot} \right] \quad ; \tag{115a}$$

$$\beta_{\mathcal{E}'} = \beta_{\mathcal{E}} \frac{\nu_{sel}^2}{\nu_{ram}} = \frac{\beta_M^5}{\beta_J^2 \beta_E} \frac{\nu_{sel}^2}{\nu_{ram}} \quad ; \tag{115b}$$

where different changes in mass, angular momentum, total energy, density profile, and rotation velocity profile, are related to the same final shape for an assigned final configuration, provided $\beta_{\mathcal{E}'}$ does not vary. The choice, $\beta_{\mathcal{E}'} = 6.007519 \cdot 10^{-6}$, in particular $(\beta_M, \beta_J, \beta_E, \nu_{sel}, \nu_{ram}) = (1, 60, 1, 0.610045, 17.20783)$, holds for Fig. 4.

5 Conclusion

With regard to homeoidally striated Jacobi ellipsoids (CM05), a unified theory of systematically rotating and peculiar motions have been developed,

where both real and imaginary rotation (around a fixed axis) have been considered. The effect of residual motion excess along the equatorial plane or the rotation axis, has been shown to be equivalent to an additional, real or imaginary rotation, respectively. Then it has been realized that a homeoidally striated Jacobi ellipsoid with assigned velocity distribution, always admits an adjoint configuration i.e. a classical Jacobi ellipsoid of equal mass and axes. In addition, further constraints have been established on the amount of residual velocity anisotropy along the principal axes, for triaxial configurations. Special effort has been devoted to investigating sequences of virial equilibrium configurations in terms of normalized parameters, including the effects of both density and velocity profile. In particular, it has been shown that bifurcation points from axisymmetric to triaxial configurations occur as in classical Jacobi ellipsoids, contrary to earlier results (Wiegandt 1982a,b; CM05). The reasons of the above mentioned discrepancy have also been explained. The occurrence of centrifugal support at the ends of equatorial major semiaxis, has briefly been discussed. An interpretation of recent results from numerical simulations on stability (Meza 2002), has been provided in the light of the model. A physical interpretation of the early Hubble sequence has shortly been reviewed and discussed from the standpoint of the model. More specifically, (i) elliptical galaxies have been considered as isolated systems, and an allowed region within Ellipsoidland (Hunter & de Zeeuw 1997), related to the occurrence of bifurcation points from ellipsoidal to pear-shaped configurations, has been shown to be consistent with observations; (ii) elliptical galaxies have been considered as embedded within dark matter haloes and, under reasonable assumptions, it has been shown that tidal effects from embedding haloes have little influence on the above mentioned results; (iii) dark matter haloes and hosted elliptical galaxies, idealized as a single homeoidally striated Jacobi ellipsoid, have been considered in connection with the cosmological transition from expansion to relaxation, by generalizing an earlier model (Thuan & Gott 1975), and the existence of a lower limit to the flattening of relaxed (oblate-like) configurations, has been established. On the other hand, no lower limit has been found to the elongation of relaxed (prolate-like) configurations, and the observed lack of elliptical galaxies more elongated than $E7$ has needed a different physical interpretation such as the occurrence of bending instabilities (Polyachenko & Shukhman 1979; Merritt & Hernquist 1991).

Acknowledgements

We are indebted to D. Merritt and V. Polyachenko for pointing our attention to their (and coauthors') papers on bending instabilities, which had been overlooked in an earlier version of the current paper.

References

[1] Bertola, F., Capaccioli, M. 1975, ApJ 200, 439

[2] Bertola, F., Galletta, G. 1978, ApJ 226, L115

[3] Bett, P. et al. 2007, MNRAS 376, 215

[4] Binney, J. 1976, MNRAS 177, 19

[5] Binney, J. 1978, MNRAS 183, 501

[6] Binney, J. 1980, MNRAS 190, 421

[7] Binney, J., & Tremaine, S. 1987, *Galactic Dynamics*, Princeton University Press, Princeton

[8] Blaauw, A. 1965, in *Stars and Stellar Systems*, vol. V, Chap. 20, § 3

[9] Brosche, P., Caimmi, R., & Secco, L. 1983, A&A 125, 338

[10] Caimmi, R. 1979, ApSS 71, 75

[11] Caimmi, R. 1983, ApSS 93, 403

[12] Caimmi, R., 1991, ApSS 180, 211

[13] Caimmi, R. 1993a, ApJ 419, 615

[14] Caimmi, R. 1993b, ApSS 199, 11

[15] Caimmi, R. 1996a, Acta Cosmologica XXII, 21

[16] Caimmi, R. 1996b, AN 317, 401

[17] Caimmi, R. 2003, AN 324, 250

[18] Caimmi, R., Secco, L., Brosche, P. 1984, A&A 139, 411

[19] Caimmi, R., Secco, L. 1992, ApJ 395, 119

[20] Caimmi, R., & Marmo, C. 2003, NewA 8, 119 (CM03)

[21] Caimmi, R., & Marmo, C. 2005, AN, submitted (CM05)

[22] Chandrasekhar, S., & Leboviz, N.R. 1962, ApJ 136, 1082

[23] Chandrasekhar, S. 1969, *Ellipsoidal Figures of Equilibrium*, Yale University Press, New Haven

[24] Durisen, R.H. 1978, ApJ 224, 826

[25] Fridman, A., Polyachenko, V.L. 1984, *Physics of Gravitating Systems*, Springer-Verlag

[26] Hernquist, L. 1990, ApJ 356, 359

[27] Hoeft, M., Mücket, J.P., Gottlöber, S. 2004, ApJ 602, 162

[28] Hubble, E. 1926, ApJ 64, 321

[29] Hunter, C., & de Zeeuw, T.Z. 1997, ApJ 389, 79

[30] Illingworth, G. 1977, ApJ 218, L43

[31] Illingworth, G. 1981, in S. M. Fall and D. Lynden-Bell (eds.), *Structure and Evolution of Normal Galaxies*, Cambridge University Press, p. 27

[32] Jeans, J. 1929, *Astronomy and Cosmogony*, Dover Publications, New York, 1961

[33] Lai, D., Rasio, F.A., & Shapiro, S.L. 1993, ApJS 88, 205

[34] Landau, L., Lifchitz, E. 1966, *Mecanique*, Mir, Moscow

[35] MacMillan, W.D. 1930, *The Theory of the Potential*, Dober Publications, New York, 1958

[36] Marochnik, L.S. 1967, Soviet Astron. AJ 10, 738

[37] Meza, A. 2002, A&A 395, 25

[38] Merritt, D., Aguilar, L.A. 1985, MNRAS 217, 787

[39] Merritt, D., Hernquist, L. 1991, ApJ 376, 439

[40] Merritt, D., Sellwood, J. 1994, ApJ 425, 551

[41] Navarro, J.F., Frenk, C.S., & White, S.D.M. 1995, MNRAS 275, 720

[42] Navarro, J.F., Frenk, C.S., & White, S.D.M. 1996, ApJ 462, 563

[43] Navarro, J.F., Frenk, C.S., & White, S.D.M. 1997, ApJ 490, 493

[44] Nipoti, C., Londrillo, P., & Ciotti, L. 2002, MNRAS 332, 901

[45] Pacheco, F., Pucacco, G., & Ruffini, R. 1986, A&A 161, 39

[46] Pacheco, F., Pucacco, G., Ruffini, R., & Sebastiani, G. 1989, A&A 210, 42

[47] Perek, L. 1962, Adv. Astron. Astrophys. 1, 165

[48] Polyachenko, V.L., Shukhman, I.G. 1979, Sov. Astr. 27, 407

[49] Raha, N., et al. 1991, Nature 352, 411

[50] Rasia, E., Tormen, G., Moscardini, L. 2004, MNRAS 351, 237

[51] Roberts, P.H. 1962, ApJ 136, 1108

[52] Roberts, M.S., Haynes, M.P. 1994, ARAA 32, 115

[53] Schechter, P.L., Gunn, J.E. 1979, ApJ 229, 472

[54] Stiavelli, M., Sparke, L.S. 1991, ApJ 382, 466

[55] Thuan, T.X., & Gott, J.R., III, 1975, Nature 257, 774

[56] van den Bergh, S. 1960a, ApJ 131, 215

[57] van den Bergh, S. 1960b, ApJ 131, 558

[58] Vandervoort, P.O., 1980a, ApJ 240, 478

[59] Vandervoort, P.O., 1980b, ApJ 241, 316

[60] Vandervoort, P.O., Welty, D.E. 1981, ApJ 248, 504

[61] Wiegandt, R., 1982a, A&A 105, 326

[62] Wiegandt, R., 1982b, A&A 106, 240

A Some properties of ellipsoid shape factors

Ellipsoid shape factors, A_1, A_2, A_3, obey the following inequalities (Caimmi 1996a):

$$a_1^n A_1 \geq a_2^n A_2 \geq a_3^n A_3 \quad ; \qquad a_1 \geq a_2 \geq a_3 \quad ; \qquad n \geq 2 \quad ; \tag{116a}$$

$$a_1^n A_1 \leq a_2^n A_2 \leq a_3^n A_3 \quad ; \qquad a_1 \geq a_2 \geq a_3 \quad ; \qquad n \leq 1 \quad ; \tag{116b}$$

where inequalities (116a) and (116b), the latter restricted to $n \leq 0$, come from analytical considerations involving the explicit expression of the shape factors (e.g., MacMillan 1930, Chap. II, § 33; $A_1 = \alpha^{-2}$, $A_2 = \beta^{-2}$, $A_3 = \gamma^{-2}$, therein), and inequality (116b), restricted to $0 < n \leq 1$, results from an obvious generalization of a proof by Pacheco et al. (1989).

Using Eqs. (6) and (7) yields:

$$\frac{\mathcal{S}_{qq}}{\mathcal{S}_{33}} = \frac{A_q}{\epsilon_{3q}^2 A_3} \quad ; \qquad q = 1, 2 \quad ; \tag{117}$$

and, owing to inequality (116a):

$$A_q \geq \epsilon_{3q}^2 A_3 \quad ; \qquad a_q \geq a_3 \quad ; \qquad q = 1, 2 \quad ; \tag{118}$$

which implies $\mathcal{S}_{qq} \geq \mathcal{S}_{33}$ for oblate-like configurations ($a_q \geq a_3$), and $\mathcal{S}_{qq} \leq \mathcal{S}_{33}$ for prolate-like configurations ($a_q \leq a_3$).

In the limit of axisymmetric configurations, $\epsilon_{21} = 1$, $\epsilon_{31} = \epsilon$, $A_1 = A_2 = \alpha$, $A_3 = \gamma$, and the following relations hold (e.g., Caimmi 1991, 1993):

$$\lim_{\epsilon \to 0} \alpha = 0 \quad ; \quad \lim_{\epsilon \to 0} \gamma = 2 \quad ; \quad \lim_{\epsilon \to 0} \frac{\alpha}{\epsilon} = \frac{\pi}{2} \quad ; \tag{119}$$

$$\lim_{\epsilon \to +\infty} \alpha = 1 \quad ; \quad \lim_{\epsilon \to +\infty} \gamma = \lim_{\epsilon \to +\infty} (\epsilon \gamma) = 0 \quad ; \quad \lim_{\epsilon \to +\infty} (\epsilon^2 \gamma) = +\infty \quad ; \tag{120}$$

$$\lim_{\epsilon \to 1} \frac{\gamma - \alpha}{1 - \epsilon^2} = \frac{2}{5} \quad ; \tag{121}$$

$$\frac{\mathrm{d}\alpha}{\mathrm{d}\epsilon} = \frac{1}{1 - \epsilon^2} \left[(1 + 2\epsilon^2) \frac{\alpha}{\epsilon} - 2\epsilon \right] \quad ; \tag{122}$$

$$\frac{\mathrm{d}\gamma}{\mathrm{d}\epsilon} = \frac{1}{1 - \epsilon^2} \left[(1 + 2\epsilon^2) \frac{\gamma}{\epsilon} - \frac{2}{\epsilon} \right] \quad ; \tag{123}$$

$$\upsilon = (\upsilon_N)_{iso} = \alpha - \epsilon^2 \gamma \quad ; \tag{124}$$

and keeping in mind the general property (e.g., Chandrasekhar 1969, Chap. 3, § 17):

$$A_1 + A_2 + A_3 = 2 \quad ; \tag{125}$$

it can be seen that the first derivative of the rotation parameter, υ, is null provided the transcendental equation:

$$\alpha = \frac{6\epsilon^2}{1 + 8\epsilon^2} \quad ; \tag{126}$$

is satisfied. One solution is found to exist, which is related to oblate configurations. It corresponds to an extremum point where the function attains its maximum value (e.g., Chandrasekhar 1969, Chap. 5, § 32), as represented in Fig. 1.

B Wiegandt criterion for bifurcation

Given a collisionless, self-gravitating fluid in rigid rotation, where no internal energy transport occurs and the residual velocity is constant on the boundary, an upper limit for the point of bifurcation is (Wiegandt 1982a,b):

$$\Omega^2 I_{11} = V_{12;12} \quad ; \tag{127}$$

where $V_{pq;rs}$ is the "super-matrix":

$$V_{pq;rs} = \int_S \rho(x_1, x_2, x_3) x_p \frac{\partial \mathcal{V}_{rs}}{x_q} \, \mathrm{d}^3 S \quad ; \tag{128}$$

$$\mathcal{V}_{rs}(x_1, x_2, x_3) = G \int_S \frac{\rho(x_1', x_2', x_3')(x_p - x_p')(x_s - x_s')}{[(x_1 - x_1')^2 + (x_2 - x_2')^2 + (x_3 - x_3')^2]^{3/2}} \, \mathrm{d}^3 S \quad ; \tag{129}$$

which is expressed in terms of a generalized potential, $\mathcal{V}_{rs}$, and the integrations are carried over the whole volume, S, of the system.

In the special case of homeoidally striated Jacobi ellipsoids, Eq. (127) identifies the exact point of bifurcation (Wiegandt 1982a,b) and the following relations hold (Wiegandt 1982b):

$$V_{pq;pq} = -\frac{A_p - a_q^2 A_{pq}}{A_p}(E_{sel})_{pp} \quad ; \tag{130}$$

$$a_q^2 A_{pq} = \frac{A_p - A_q}{1 - \epsilon_{pq}^2} \quad ; \tag{131}$$

where the products, $a_q^2 A_{pq}$, are shape factors which depend on the axis ratios only, similarly to A_p, and symmetry with respect to the indices holds, $A_{pq} = A_{qp}$. In addition, Eq. (131) has been deduced from Chandrasekhar (1969, Chap. 3, § 21), Eq. (107) therein.

Though Wiegandt (1982b) analysis is restricted to binomial density profiles (e.g., Perek 1962; Chandrasekhar 1969, Chap. 3, § 20; Caimmi 1993), still it may be generalized to any kind of cored density profiles, defined as:

$$\rho_W(\xi) = \rho_c f(\xi_W) \quad ; \qquad f(0) = 1 \quad ; \qquad \rho_c = \rho(0) \quad ; \tag{132a}$$

$$\xi_W = \frac{r}{R} \quad ; \qquad 0 \leq \xi_W \leq 1 \quad ; \qquad \Xi_W = 1 \quad ; \tag{132b}$$

where the scaling radius and the scaling density are chosen to be equal to the radius, R, and the central density, ρ_c, respectively. The following relations:

$$\rho = \frac{\rho_0}{\rho_c}\rho_W \quad ; \qquad \xi = \Xi\xi_W \quad ; \tag{133}$$

allow conversion from Eqs. (1) to Eqs. (132) and vice versa.

Using Eqs. (132), the mass, the inertia tensor, and the potential-energy tensor, take the equivalent expression:

$$M = (\nu_{mas})_W M_c \quad ; \tag{134a}$$

$$M_c = \frac{4\pi}{3}\rho_c a_1^3 \epsilon_{21}\epsilon_{31} \quad ; \tag{134b}$$

$$I_{pq} = \delta_{pq}\epsilon_{p1}\epsilon_{q1} a_1^2 M(\nu_{inr})_W \quad ; \tag{135}$$

$$(E_{sel})_{pq} = -(\nu_{sel})_W \frac{GM^2}{a_1}(B_{sel})_{pq} \quad ; \tag{136}$$

and the comparison with Eqs. (2), (3), (4), (8), yields:

$$(\nu_{mas})_W = \frac{\rho_0}{\rho_c}\frac{1}{\Xi^3}\nu_{mas} \quad ; \qquad (\nu_{inr})_W = \nu_{inr} \quad ; \qquad (\nu_{sel})_W = \nu_{sel} \quad ; \tag{137}$$

finally, using Eqs. (6) and (134)-(137), the potential-energy tensor takes the equivalent form:

$$(E_{sel})_{pq} = -k\pi G\rho_c I_{pq} A_p \quad ; \tag{138a}$$

$$k = \frac{4}{3}\frac{\rho_0}{\rho_c}\frac{\nu_{sel}\nu_{mas}}{\Xi^3\nu_{inr}} \quad ; \tag{138b}$$

being k, by definition, a profile factor.

Owing to Eqs. (8), (18), (20), (34), (35), (138b), the normalized rotation parameter, defined by Eq. (48), may be expressed as:

$$\upsilon_N = \frac{\Omega^2}{k\pi G\rho_c} \quad ; \tag{139}$$

which coincides with the parameter, ϕ, defined in Wiegandt (1982b), as shown in Caimmi (1996b). Accordingly, Eq. (49) coincides with its Wiegandt (1982b) counterpart, Eq. (52) therein.

The combination of Eqs. (127), (130), (138), (139), yields:

$$\upsilon_N = A_1 - a_2^2 A_{12} \quad ; \tag{140}$$

and the comparison with Eq. (49) reads:

$$a_2^2 A_{12} = \frac{\zeta_{11}}{\zeta_{33}}\epsilon_{31}^2 A_3 \quad ; \tag{141}$$

in the limit of axisymmetric configurations, $a_2 \to a_1$, $A_{12} \to A_{11}$, the left-hand side of Eq. (141) takes the expression (e.g., Caimmi 1993):

$$\lim_{a_2 \to a_1} a_2^2 A_{12} = \frac{1}{4}\left(3A_1 - \epsilon_{31}^2 \frac{A_3 - A_1}{1 - \epsilon_{31}^2}\right) \quad ; \tag{142}$$

and the combination of Eqs. (141), (142), yields:

$$\frac{\epsilon_{31}^2 A_3}{A_1} = \left[\frac{5 - 4\epsilon_{31}^2}{3 - 2\epsilon_{31}^2} + \frac{4(1 - \epsilon_{31}^2)}{3 - 2\epsilon_{31}^2}\frac{\zeta_{11} - \zeta_{33}}{\zeta_{33}}\right]^{-1} \quad ; \qquad \epsilon_{21} = 1 \quad ; \tag{143}$$

which is an explicit expression of Wiegandt (1982a,b) criterion for bifurcation, with regard to homeoidally striated Jacobi ellipsoids in rigid rotation. In the limit of isotropical residual velocity distribution, $\zeta_{11} = \zeta_{22} = \zeta_{33}$, Eq. (143) reduces to (65), as expected.

The condition, defined by Eq. (143), has to be compared with its counterpart deduced in the current paper, under the same assumption i.e. $\zeta_{11} = \zeta_{22}$ also for triaxial configurations. The latter may be deduced from Eq. (84), using the relation (e.g., Caimmi 1966a):

$$\lim_{\epsilon_{21} \to 1} \epsilon_{21}^2 \frac{A_2 - A_1}{1 - \epsilon_{21}^2} = \frac{1}{4} \left(3A_1 - \epsilon_{31}^2 \frac{A_3 - A_1}{1 - \epsilon_{31}^2} \right) \quad ; \tag{144}$$

and the result is again Eq. (143). Then Wiegandt (1982b) criterion for bifurcation can be deduced from the current theory, provided isotropic residual velocity distribution is assumed along the equatorial plane, also for triaxial configurations. On the other hand, the above assumption is in contradiction with Eqs. (63) and then it cannot be accepted. A criterion for bifurcation, consistent with Eqs. (63), is expressed by Eq. (65).

The origin of the discrepancy could be the following. Wiegandt (1982a) assumption (ii) implies Eq. (12) therein which, after integration, yields isotropic residual velocity distribution along the equatorial plane i.e. $\zeta_{11} = \zeta_{22}$. On the other hand, an isotropic residual velocity distribution along the equatorial plane is related to a zero-th order approximation in some special series developments [Marochnik 1967; Eq. (19) therein]. The additional requirement of axial symmetry makes the above mentioned relation be exact, but in presence of triplanar symmetry it has to be considered as a zero-th order approximation.

In the light of the results discussed in the current subsection, the analogy between the behaviour of collisional and collisionless self-gravitating fluids, subjected to the restrictions (Wiegandt 1982a,b): (i) rigid rotation; (ii) constant residual velocity on the boundary; (iii) absence of internal energy transports; appears to be complete.